Ancient origin of the rod bipolar cell pathway in the vertebrate retina

Ayana M Hellevik[1,*], Philip Mardoum[1,*], Joshua Hahn[2,*], Yvonne Kölsch[3,4], Florence D D'Orazi[1], Sachihiro C. Suzuki[1], Leanne Godinho[5], Owen Lawrence[1], Fred Rieke[6,7], Karthik Shekhar[2,8], Joshua R Sanes[3], Herwig Baier[4], Tom Baden[9,10], Rachel O Wong[1], Takeshi Yoshimatsu[11,12,#]

1, Department of Biological Structure, University of Washington, Seattle, WA 98195, USA; 2, Department of Chemical and Biomolecular Engineering; Helen Wills Neuroscience Institute; Vision Sciences Graduate Program; California Institute of Quantitative Biosciences (QB3), University of California Berkley, Berkeley, CA 94720, USA; 3, Department of Molecular & Cellular Biology and Center for Brain Science, Harvard University, Cambridge, MA 02138, USA; 4, Max Planck Institute for Biological Intelligence, Department Genes – Circuits – Behavior, 82152 Martinsried, Germany; 5, Institute of Neuronal Cell Biology, Technische Universität München, 80802 Munich, Germany; 6, Department of Physiology and Biophysics, University of Washington, Seattle, WA 98195, USA; 7, Vision Science Center, University of Washington, Seattle, WA 98195, USA; 8, Biological Systems and Engineering Division, Lawrence Berkeley National Laboratory, Berkeley, CA 94720, USA; 9, School of Life Sciences, University of Sussex, Brighton, BN1 9QG, UK; 10, Institute of Ophthalmic Research, University of Tübingen, Tübingen, 72076, Germany; 11, Department of Ophthalmology & Visual Sciences, Washington University in St Louis School of Medicine, St Louis, MO 63110, USA; 12, BioRTC, Yobe State University, Damatsuru, Yobe 620101, Nigeria

*These authors contributed equally to this study

24 #Lead contact: Takeshi Yoshimatsu takeshi@wustl.edu

25

26 **Keywords**

27 Rod, Rod bipolar cells, Retina, Evolution

28

29 **Highlights**

30 - Zebrafish have two rod bipolar cell types (RBC1/2).
31 - Synaptic connectivity of RBC1 resembles that of the mammalian RBCs.
32 - The primary rod pathway therefore probably evolved more than 400 million years ago.
33 - The second zebrafish RBC type, RBC2, forms a separate pathway from RBC1.

34

ABSTRACT

Vertebrates rely on rod photoreceptors for vision in low-light conditions[1]. Mammals have a specialized downstream circuit for rod signaling called the primary rod pathway, which comprises specific cell types and wiring patterns that are thought to be unique to this lineage[2–6]. Thus, it has been long assumed that the primary rod pathway evolved in mammals[3,5–7]. Here, we challenge this view by demonstrating that the mammalian primary rod pathway is conserved in zebrafish, which diverged from extant mammals ~400 million years ago. Using single-cell RNA-sequencing, we identified two bipolar cell (BC) types in zebrafish that are related to mammalian rod BCs (RBCs) of the primary rod pathway. By combining electrophysiology, histology, and ultrastructural reconstruction of the zebrafish RBCs, we found that, like mammalian RBCs[8], both zebrafish RBC types connect with all rods and red-cones in their dendritic territory, and provide output largely onto amacrine cells. The wiring pattern of the amacrine cells post-synaptic to one RBC type is strikingly similar to that of mammalian RBCs. This suggests that the cell types and circuit design of the primary rod pathway may have emerged before the divergence of teleost fish and amniotes (mammals, bird, reptiles). The second RBC type in zebrafish, which forms separate pathways from the first RBC type, is either lost in mammals or emerged in fish to serve yet unknown roles.

52 **INTRODUCTION**

53 Rod photoreceptors of the vertebrate retina are capable of detecting very dim light, down to
54 individual photons[9–14]. The mammalian cell types and circuitry that convey rod-driven signals,
55 called the primary rod pathway, were identified and defined in the cat retina about 50 years ago[15].
56 Since its initial characterization, this rod pathway has been examined extensively in many
57 mammalian species including in humans, where it consistently uses homologous cell types and
58 connectivity patterns: Rod bipolar cells (RBCs), as well as A2 and A17 amacrine cells[3,5,6,16,17]. The
59 RBC is a molecularly, structurally and functionally distinct retinal bipolar cell type that receives
60 input from all rods within its dendritic field and is predominantly driven by rods[8,18–21]. In mammals,
61 all other bipolar cell types receive most of their photoreceptor input from cones, which operate in
62 daylight conditions. In contrast, the bipolar cells that have been characterized in non-mammals
63 lack clear distinctions regarding the ratio of rod and cone inputs[14,22]. Thus, it is not surprising that
64 the RBC is thought to be unique to mammals, a notion that has led to the prevailing view that the
65 rod pathway evolved separately in this class[3,5–7]. However, the molecular, structural and functional
66 signatures that together define bipolar cell types in mammals are largely unknown in non-
67 mammals, so it remains unclear whether the signatures characteristic of the mammalian RBC
68 and its downstream pathway are present in non-mammals. To address this issue, we focused on
69 zebrafish, a species that allows transgenic labeling of neuronal populations, to analyze single-cell
70 transcriptomics, histology, physiology and circuit reconstructions of genetically-defined retinal
71 bipolar cells.

72 There are more than a dozen BC types in mammals that are diverse in morphology, connectivity
73 and molecular profiles[23–27], but can be classified into two main groups: ON BCs that depolarize
74 and OFF BCs that hyperpolarize in response to increases in luminance[28]. RBCs are one type of
75 ON BCs that are distinct in many ways from all other BCs, which mainly connect with cones and
76 are called cone BCs (CBCs) here. Transcriptionally, mammalian RBCs can be distinguished from

77 CBCs by the expression of protein kinase C-alpha (PKCα)[29]. Morphologically, the axon terminals
78 of RBCs are generally larger than those of CBCs and end in the innermost layer of the inner
79 plexiform layer (IPL). The synaptic arrangement of the RBC axons differs from the common
80 synaptic arrangement of most cone bipolar cells. Whereas CBC axons directly synapse onto the
81 retinal output neurons, retinal ganglion cells (RGCs), along with a plethora of amacrine cells (ACs),
82 RBCs predominately form a 'dyadic' synapse with two types of inhibitory amacrine cells, small
83 field A2 (or A-II) and large-field A17 ACs[15,18,19,30]. The A17 AC almost exclusively makes reciprocal
84 feedback synapses onto RBC axon terminals[31]. In contrast, A2 ACs receive numerous synapses
85 from RBCs (~40 synapses per RBC in mice), but do not provide feedback onto the RBCs[18,32].
86 These RBC to A2 AC synapses are the critical sites for the amplification and gain control of rod
87 signals[33–35]. Rod signals are eventually relayed to RGCs by connections from A2 ACs on CBCs,
88 which split rod signals into ON and OFF channels via sign-conserving gap junctions with ON
89 CBCs and inhibitory synapses with OFF CBCs[15,36,37].

90 Here, by analyzing single-cell transcriptomic profiles of zebrafish BCs, we discovered two BC
91 types, RBC1 and RBC2, with molecular signatures similar to those of mammalian RBCs. Using
92 transgenic zebrafish lines that express a fluorescent protein in RBC1 or RBC2 cells, we identified
93 the inputs and outputs of RBC1 and RBC2. We found that both zebrafish RBC types connect with
94 all rods and red cones (or longwave-length sensitive, LWS, cones) inside their dendritic fields.
95 We further reconstructed the downstream circuits of both BC types using serial block-face
96 electron microscopy and found that RBC1 predominantly synapses onto three morphological
97 types of ACs. The circuit diagrams and synaptic arrangements of two of the ACs closely resemble
98 those of the mammalian A2 and A17 ACs. In contrast, RBC2 mainly connects to a different set of
99 ACs, which does not include A2-like ACs. These results suggest that (i) zebrafish possess two
100 separate pathways for processing rod signals, and that (ii) one of these is similar to the rod –>
101 RBC –> A2 AC –> CBC –> RGC pathway found in mammals. We conclude that the primary rod

102 pathway emerged >400 million years ago, before the divergence of teleosts and mammals in the
103 Devonian.

104

105 **RESULTS**

106 **Two zebrafish BC types are transcriptionally analogous to the mammalian RBCs**

107 We first determined the transcriptional similarity between each zebrafish BC type and the
108 mammalian RBCs by using single-cell RNA-sequencing (scRNA-seq) in adult zebrafish. BCs
109 were isolated using a fluorescent marker in the *Tg(vsx1:GFP)*^{nns5} transgenic line, in which all BCs
110 express GFP[38] (Fig. 1a). Clustering analysis of 19492 high-quality single cell transcriptomes
111 identified 23 molecularly distinct BC clusters (Fig. 1b,c). To identify the clusters most similar to
112 mammalian RBCs, we performed a hierarchical clustering analysis based on average
113 transcriptomic profiles (Fig. 1d) and combined this with the expression patterns of marker genes
114 identified in mice to tentatively annotate each cluster as ON CBC, OFF CBC or RBC (Fig. 1e; [27]).
115 In mice, RBCs are clearly separated from CBCs at the first dendrogram bifurcation[27]. Similarly,
116 the first dendrogram bifurcation separates two BCs from the other BCs in zebrafish. In contrast to
117 mice, however, the zebrafish RBC clade contained two molecularly distinct clusters 14 (c14) and
118 19 (c19) (Fig. 1d). We observed that *prkca* (the gene encoding PKCα), a common marker of
119 mammalian RBCs, is only highly expressed in c14. However, both c14 and c19 specifically
120 express *gramd1b*, which is an RBC-specific marker in mice. In addition to these genetic
121 signatures similar to mammalian RBCs, both c14 and c19 clusters express neurotransmitter
122 receptor, *grm6a* and *grm6b,* and it's downstream signaling molecules, *trpm1a, trpm1b*, *nyx* and
123 *rgs11,* which are essential for mediating rod inputs in mammals[39] (Fig. S1). Therefore, we
124 hypothesized that zebrafish, unlike mice, may possess two RBC types, which we call RBC1 (c14)
125 and RBC2 (c19).

Figure 1

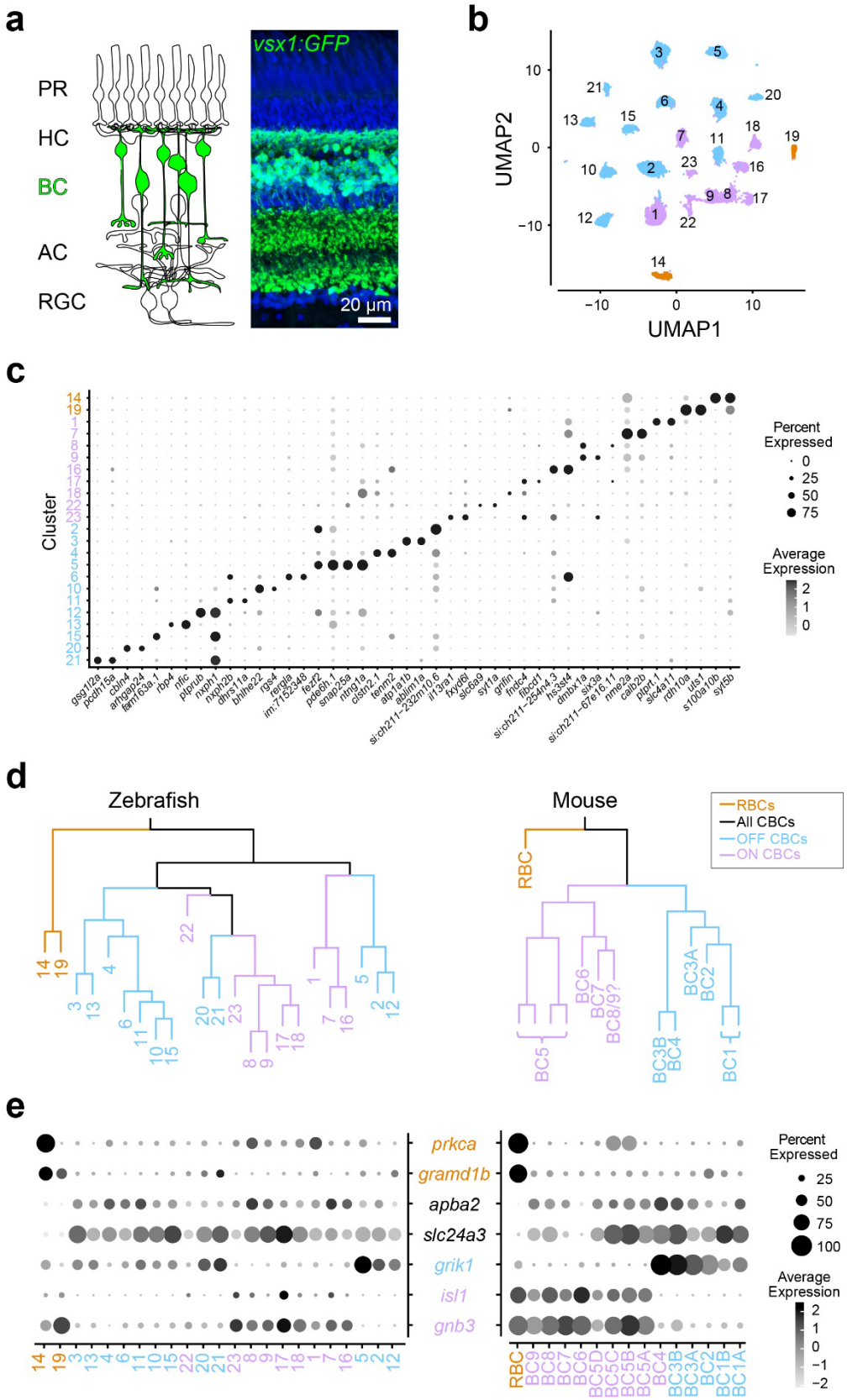
a
PR
HC
BC
AC
RGC
vsx1:GFP
20 µm
b
UMAP2
UMAP1
c
Cluster
Percent Expressed
Average Expression
d
Zebrafish
Mouse
RBCs
All CBCs
OFF CBCs
ON CBCs
e
prkca
gramd1b
apba2
slc24a3
grik1
isl1
gnb3
Percent Expressed
Average Expression

127 ***Figure 1. Comparison of single-cell gene expressions identified two possible rod bipolar***
128 ***cells in zebrafish***

129 ***a,*** *Schematic representation of retinal circuits (left) and an image of a retinal slice from*
130 *Tg(vsx1:GFP)^{nns5} transgenic adult zebrafish (right). GFP expression in all bipolar cells (BCs).*
131 *Nuclei was stained by DAPI. PR: photoreceptor, HC: horizontal cell, AC: amacrine cell, RGC:*
132 *retinal ganglion cell.* ***b****, 2D visualization of single-cell clusters using Uniform Manifold*
133 *Approximation (UMAP)*[40]*. Individual points correspond to single cells colored according to cluster*
134 *identity.* ***c****, Marker genes for each cluster.* ***d****, Agglomerative hierarchical clustering of average*
135 *gene signatures of clusters using the correlation metric and complete linkage. BC subclasses*
136 *(colors) were assigned based on the known marker expressions shown in* ***e****.* ***e****, Gene expression*
137 *patterns of known BC subclass markers in BC clusters. The size of each circle depicts the*
138 *percentage of cells in the cluster in which the marker was detected (≥1 UMI), and its contrast*
139 *depicts the scaled average expression level of cells within the cluster in* ***c,e****. Data for mouse is*
140 *from Shekhar K, et al., 2016, Cell.*

Figure S1

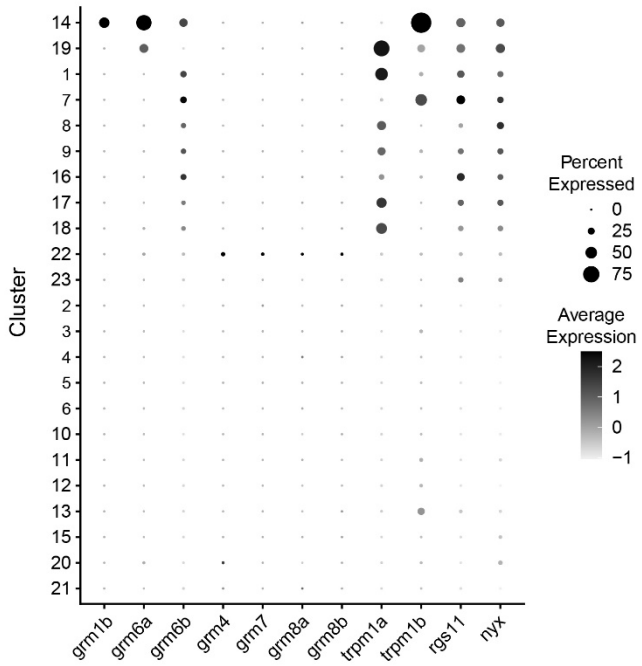

Figure S1. Expression patterns of the identified marker genes in BC clusters

The size of each circle depicts the percentage of cells in the cluster in which the marker was detected (≥1 UMI), and its grey scale depicts the scaled average expression level of cells within the cluster

151 **RBC1 and RBC2 morphologies resemble mammalian RBCs**

152 We next determined the morphological similarities of RBC1 and RBC2 with mammalian RBCs. In
153 mammals, RBC axons arborize in the innermost layer of the IPL[40]. By screening our zebrafish
154 transgenic lines, we identified two lines, *Tg(vsx1:memCerulean)*^{q19} (*vsx1:memCer)* and
155 *Tg(vsx2:memCerulean)*^{wst01} (*vsx2:memCer)*, that each label BCs with axon terminals in the
156 innermost layer of the IPL (Fig. 2). Fluorescent *in situ* hybridization for the identified gene markers,
157 *s100a10b* and *uts1,* which are selectively expressed by RBC1 and RBC2 (Fig. 1c), revealed that
158 *vsx1:memCer* and *vsx2:memCer* label RBC1 and RBC2, respectively (Fig. 2a,b). We also
159 observed that dendritic arbors of both RBC1 and RBC2 cover the retina in a non-overlapping
160 manner, an arrangement called 'tiling' that is considered a hallmark of a BC type (Fig. 2e,f)[41].
161 Therefore, both RBC1 and RBC2 represent single bipolar types that transcriptionally and
162 morphologically resemble mammalian RBCs.

163 We observed slight variations in morphology and molecular expression between RBC1 and RBC2.
164 The axon terminal of RBC1 is relatively spherical, similar to mammalian RBCs, in contrast to the
165 'flat-footed' axonal ending of RBC2 (Fig. 2c,d). RBC1 were immunoreactive for PKCα (Fig. 2c),
166 whereas RBC2 were not (Fig. 2d), consistent with the difference in their *prkca* expression (Fig.
167 1d). In addition, their abundance differed: RBC1s were more densely packed than RBC2s
168 (*p=0.0052*, Mann-Whitney two-tailed U test) (Fig. 2g,i). This difference in the densities is unlikely
169 due to regional variations as both RBCs are present in the dorsal and ventral-temporal retina at
170 similar densities (Fig. 2g,i and Fig. S2). The dendritic field sizes of the two RBC types were
171 inversely related to their cell density, consistent with their tiling arrangement (Fig. 2g-j).

172

173

174

Figure 2

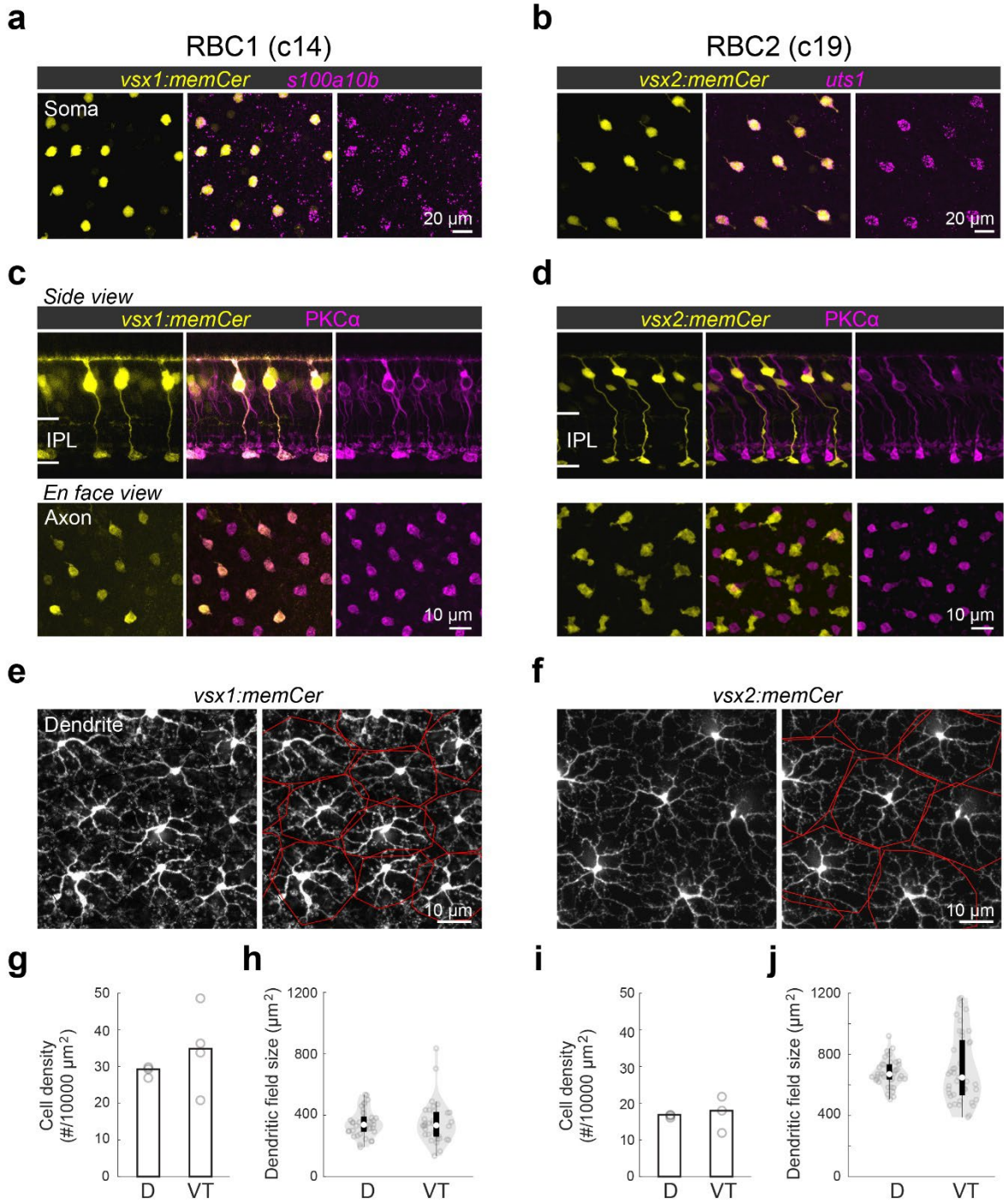

Figure 2. Transgenic labeling of cluster 14 and 19 revealed morphological features of these BCs

a,b, *En face view of retinal flat mount at the inner nucleus layer level. Cerulean fluorescent expression (colored yellow) transgenic lines, Tg(vsx1:memCerulean)^{q19} (vsx1:memCer) in* ***a*** *and*

179 *Tg(vsx2:memCerulean)^{wst01} (vsx2:memCer) in **b**. vsx1:memCer and vsx2:memCer BCs are*
180 *positive for cluster specific genes, s100a10b and uts1, respectively, which are detected using in*
181 *situ hybridization chain reaction* [43]. ***c,d**, Side views of the labeled cells and the distribution patterns*
182 *of their axon terminals in en face views of retinal flat mounts for RBC1 (**c**) and RBC2 (**d**) BCs.*
183 *Immunolabeling for PKCα is in magenta. IPL: inner plexiform layer. Note that not all PKC-*
184 *immunoreactive cells are apparent in this image of the vsx1:memCer line, due to the incomplete*
185 *labeling of this line. **e,f**, Dendritic tiling of RBC1 (**e**) and RBC2 (**f**) in en face view of retinal flat*
186 *mounts at the outer plexiform layer level. Dendritic territories are marked by the red boundaries.*
187 ***g-j**, Mean cell densities of RBC1 (**g**, n=3 and 4 for D and VT, respectively) and RBC2 (**I**, n=3 for*
188 *both D and VT) BCs in different regions of the retina. Box and violin plots of dendritic field sizes*
189 *of RBC1 (h, n=37 and 33 or D and VT, respectively) and RBC2 (j, n=40 and 41 or D and VT,*
190 *respectively) BCs. White filled circles are medians. Grey circles indicate individual cells. D: dorsal,*
191 *VT: ventrotemporal.*

Figure S2

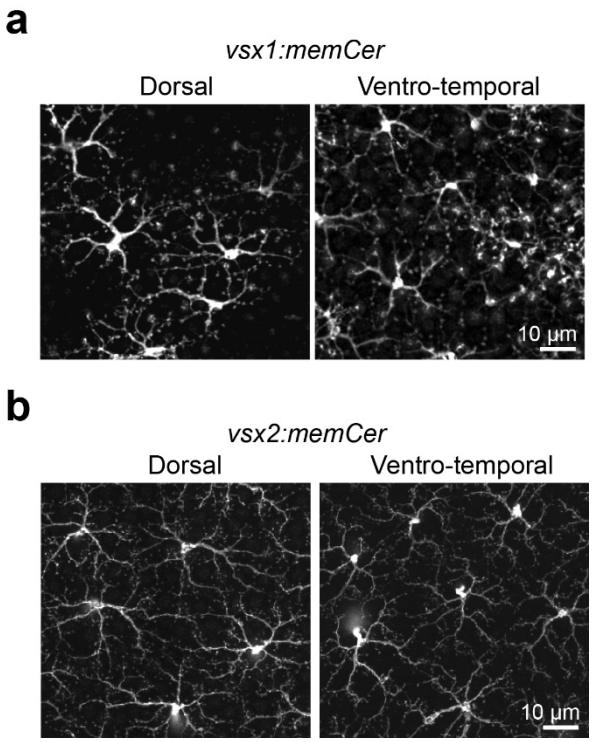

Figure S2. Dendritic tiling of RBC1 and RBC2 BCs across the retina

Confocal images of retinal flat mount at outer plexiform layer level from Tg(vsx1:memCerulean)^{q19} (vsx1:memCer) and Tg(vsx2:memCerulean)^{wst01} (vsx2:memCer). Note that the vsx1:memCer line occasionally labels OFF BCs. These BCs were distinguished by tracing the cells to the axon terminals in the confocal image volumes.

203 **Both RBC1 and RBC2 connect with all rods and red-cones in their dendritic territory**

204 If RBC1 and RBC2 are authentic RBCs, they should synapse preferentially with rods. Using 4C12
205 antibodies to label rods, we found that the majority of the dendritic tips of both RBC types (RBC1:
206 84±3.9%, RBC2: 78±2.9%) contacted with rod spherules (Fig. 3a-d). We also found that some
207 dendritic tips were not associated with rods (Fig. 3a-d). Using transgenic lines to label specific
208 cone types, we identified that dendritic tips of both BC types contacted red-cones (or long-
209 wavelength sensitive cones), labeled in the *Tg(trb2:tdtomato)*^{q22} line (Fig. 3a-e,g). Furthermore,
210 both types connected with nearly all rods and red cones within their dendritic fields (Fig. 3f,h). We
211 did not observe any dendritic tips that were not associated with either rods or red cones (Fig.
212 3e,g), indicating that they receive few if any inputs from the other cone types, which include green,
213 blue, and violet cones[42,43]. Therefore, both RBC1 and 2 receive predominant rod input and share
214 specificity for red cones among cones (Fig. 3e,g).

215 Interestingly, the dendritic tips of RBC1 and RBC2 terminating in rod spherules differed in
216 structure (Fig. 3c,d). Specifically, the dendrites of RBC1 invaginating rod spherules appeared to
217 form a horseshoe or 'doughnut' ending, whereas those of RBC2 ended in a simpler arrangement
218 (Fig. 3c,d). The larger surface area of RBC1's dendritic tips at rod terminals may increase the
219 sensitivity to rod inputs in this BC type compared to RBC2. We also observed differences in the
220 distal axonal boutons of RBC1 and RBC2 (Fig. 3i,j). While axons of both types terminate close to
221 the ganglion cells in the IPL, RBC2 axons have a bouton in the OFF layer of the IPL, next to the
222 boundary with the ON layer (Fig. 3j). These distal boutons are likely pre-synaptic sites as they
223 contain the pre-synaptic protein, Ribeye (Fig. 3j). These differences in the dendritic tip and axon
224 bouton shapes between RBC1 and RBC2 suggest that, while both BCs receive input from the
225 same combination of photoreceptor types, they may serve distinct visual functions.

226

Figure 3

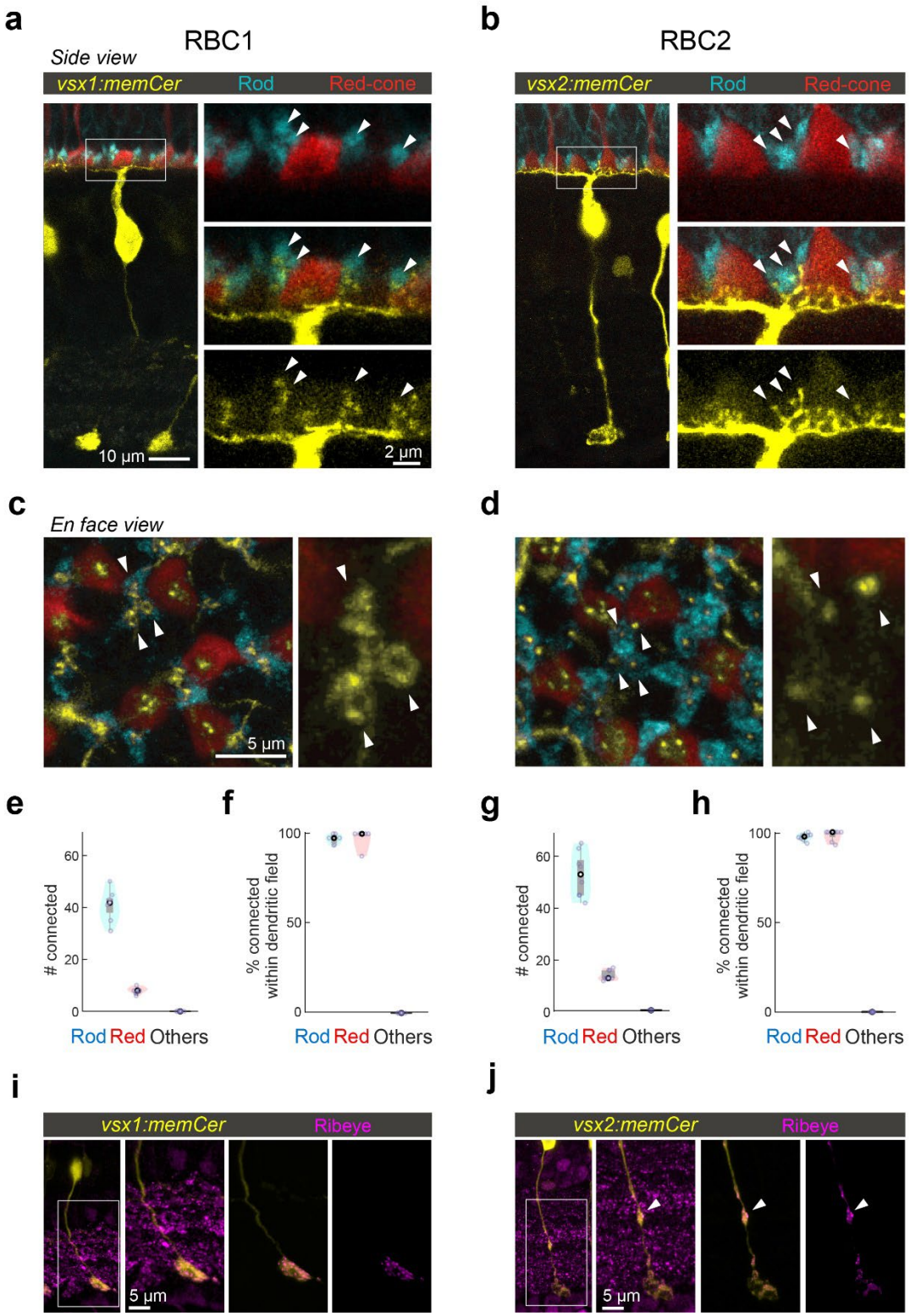
a
RBC1
Side view
vsx1:memCer
Rod
Red-cone
10 µm
2 µm
b
RBC2
vsx2:memCer
Rod
Red-cone
c
En face view
5 µm
d
e
connected
Rod Red Others
f
% connected within dendritic field
Rod Red Others
g
connected
Rod Red Others
h
% connected within dendritic field
Rod Red Others
i
vsx1:memCer
Ribeye
5 µm
j
vsx2:memCer
Ribeye
5 µm

227

228 ***Figure 3. RBC1 and RBC2 connect to rods and red cones but differ in dendritic and axonal***
229 ***synaptic arrangements***

230 ***a,b****, Dendritic tips invaginating the rod and red cone axon terminals, visualized in retinal slices*
231 *from (a) Tg(vsx1:memCerulean:trb2:tdtomato)^{q19,q22} and (b)*
232 *Tg(vsx2:memCerulean:trb2:tdtomato)^{wst01,q22} adult zebrafish. Rods were immunolabeled using*
233 *4C12 antibody.* ***c,d****, Doughnut and simple dendritic tip structures at rod terminals (arrow heads)*
234 *in RBC1 and RBC2, respectively.* ***e-h****, Box and violin plots of RBC1 (****e,f****, n=7) and RBC2 (****g,h****,*
235 *n=8) connectivity with photoreceptors.* ***i,j****, Distribution of ribbon synapses in the RBC1 (****i****) and 2*
236 *(****j****) axons. Ribbons were immunolabeled by anti-ribeye antibody. Ribeye signals outside the axons*
237 *were digitally masked out in the right two images. RBC2 axon harbors a ribbon containing distal*
238 *bouton in the OFF layer (arrow head).*

239

240 **RBC1 receives rod inputs via mGluR6 receptors**

241 We next asked whether zebrafish RBCs receive functional rod input via the metabotropic
242 glutamate receptor mGluR6 as seen in mammalian RBCs. We first investigated the expression of
243 mGluR6 in RBC1 and RBC2 dendritic tips at rod spherules. Super-resolution imaging of mGluR6
244 immunolabeling in *vsx1:memCerulean and vsx2:memCerulean* retinas showed that the dendritic
245 tips of RBC1, but not RBC2, robustly overlapped with mGluR6 immunoreactivity at contacts with
246 rod spherules (Fig. 4a,b). These findings are consistent with the transcriptional profiles, which
247 showed that RBC1 expresses higher mRNA levels of *grm6a* and *grm6b*, which encodes mGluR6,
248 than RBC2 (Fig. S1).

249 We then used electrophysiological recordings to ask whether mGluR6 mediates rod input to the
250 zebrafish RBCs. We prepared retinal wholemounts that preserve synaptic connections in the
251 outer retina, and performed whole-cell patch-clamp recordings on the axon terminals of RBC1

252 and RBC2 (Fig. 4c). Both RBC1 (n = 10) and RBC2 cells (n = 3) exhibited ON responses to a
253 cone-activating flash (red LED), confirming the successful patch-clamp recordings of light
254 responses in these BCs and demonstrating that both cell types are ON cells (Fig. 4d), consistent
255 with the position of their axonal arbors (Fig. 2c,d).

256 Although measuring rod-mediated responses from RBC2 was infeasible for technical reasons
257 (see Methods), we were successful in recording rod responses from RBC1. We were therefore
258 able to ask whether these responses mediated by mGluR6. We presented rod-isolating dim blue
259 flashes (10 ms) before and after introducing the mGluR6 receptor agonist 6-(2-
260 aminopropyl)benzofuran (APB) to the perfusion solution. To isolate excitatory inputs to the cell,
261 all recordings were performed near the reversal potential for chloride-mediated conductances (~-
262 60 mV) and in the presence of inhibitory receptor blockers, gabazine, strychnine, and TPMPA
263 ((1,2,5,6-Tetrahydropyridin-4-yl)methylphosphinic acid). Our results showed that nearly all rod
264 inputs were blocked in the presence of APB, indicating that, like mammalian RBCs, mGluR6
265 mediates rod input to RBC1 (Fig. 4e).

266

267 **Both RBCs primarily synapse onto amacrine cells**

268 To determine the synaptic targets of RBC1 and RBC2, we reconstructed their connectomes using
269 serial block face scanning electron microscopy (SBFSEM). In the reconstructions, we observed
270 an array of large BC axon terminals in the innermost layer of the IPL, which are characteristics of
271 RBC1 and RBC2 axons (Fig. S3a,b). To confirm that these large axon terminals belong to RBC1
272 and RBC2, we reconstructed dendrites of some of these BCs (Fig. 5a). Consistent with our
273 observations in light microscopic experiments (Fig. 3a-d), the large axon BCs predominantly
274 connect with rods.

275

Figure 4

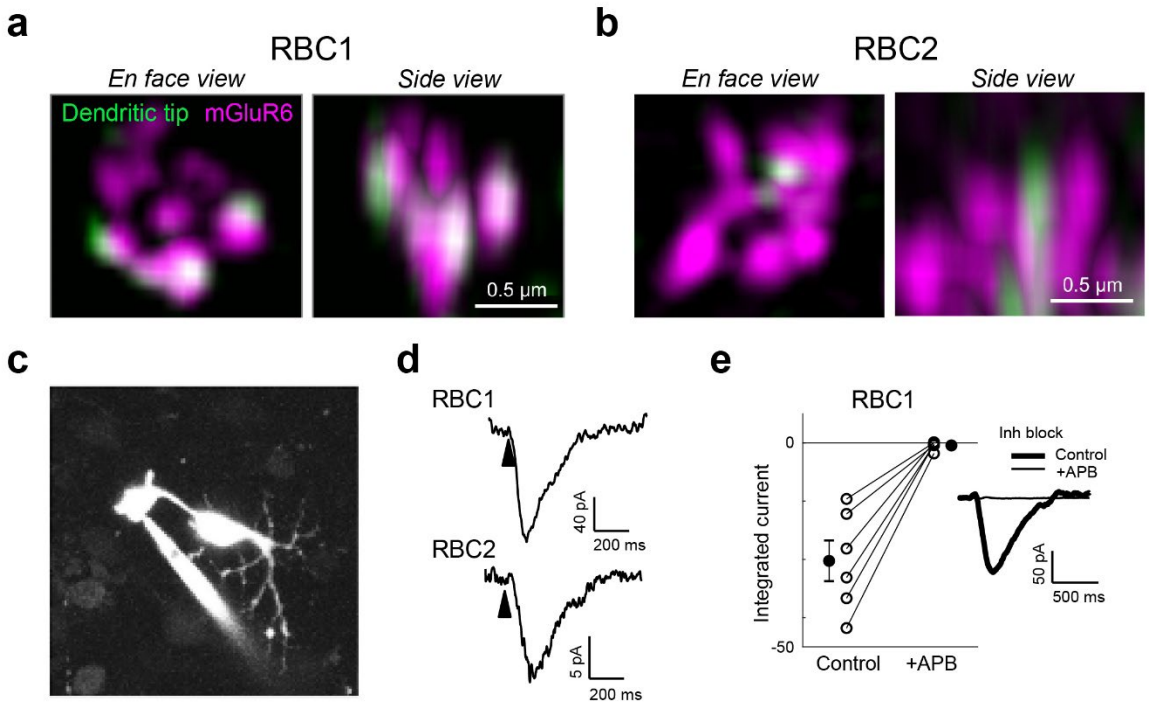

276

277 ***Figure 4. Rod input to RBC1 is mediated by mGluR6 receptors.***

278 ***a,b****, Colocalization of mGluR6 and RBC1 (**a**) and RBC2 (**b**) dendritic tips at rod terminals*
279 *visualized by structured illumination microcopy. **c**, Whole-cell patch clamping of a RBC1 axon*
280 *terminal, visualized by dye-filling Alexa Fluor 594). **d**, Voltage responses of RBC1 and RBC2 after*
281 *a cone activating light flash (arrow heads). **e,** Population data of RBC1 responses to rod activating*
282 *light flashes with and without the group III metabotropic glutamate receptor agonist, APB (6-(2-*
283 *aminopropyl)benzofuran). Filled circles: mean; error bars, S.D.; open circles, individual cells.*
284 *Traces on the right are an example of the cell's light evoked response before and during APB*
285 *bath application. Inhibitory neurotransmitter receptors were blocked (inh lock) by a bath*
286 *application of gabazine, strychnine, and TPMPA ((1,2,5,6-Tetrahydropyridin-4-*
287 *yl)methylphosphinic acid).*

288 We then reconstructed all the large axons in the SBFSEM image volume. To distinguish RBC2
289 from RBC1, we used the ribbon containing axonal distal bouton in the OFF layer as a proxy for
290 RBC2 (Fig. 3i,j and Fig. 5b). These reconstructions revealed the regular mosaic arrangements of
291 both presumed RBC1 and RBC2 (Fig. 5c), indicating that we identified most, if not all, presumed
292 RBC1 and RBC2 in the EM volume. Using this criterion, we also verified that dendritic tips of
293 RBC1 are doughnut shaped whereas those of RBC2 ended in a simple tip within the rod spherule,
294 consistent with our light microscopy data (Fig. 3c,d, 5a).

Figure 5

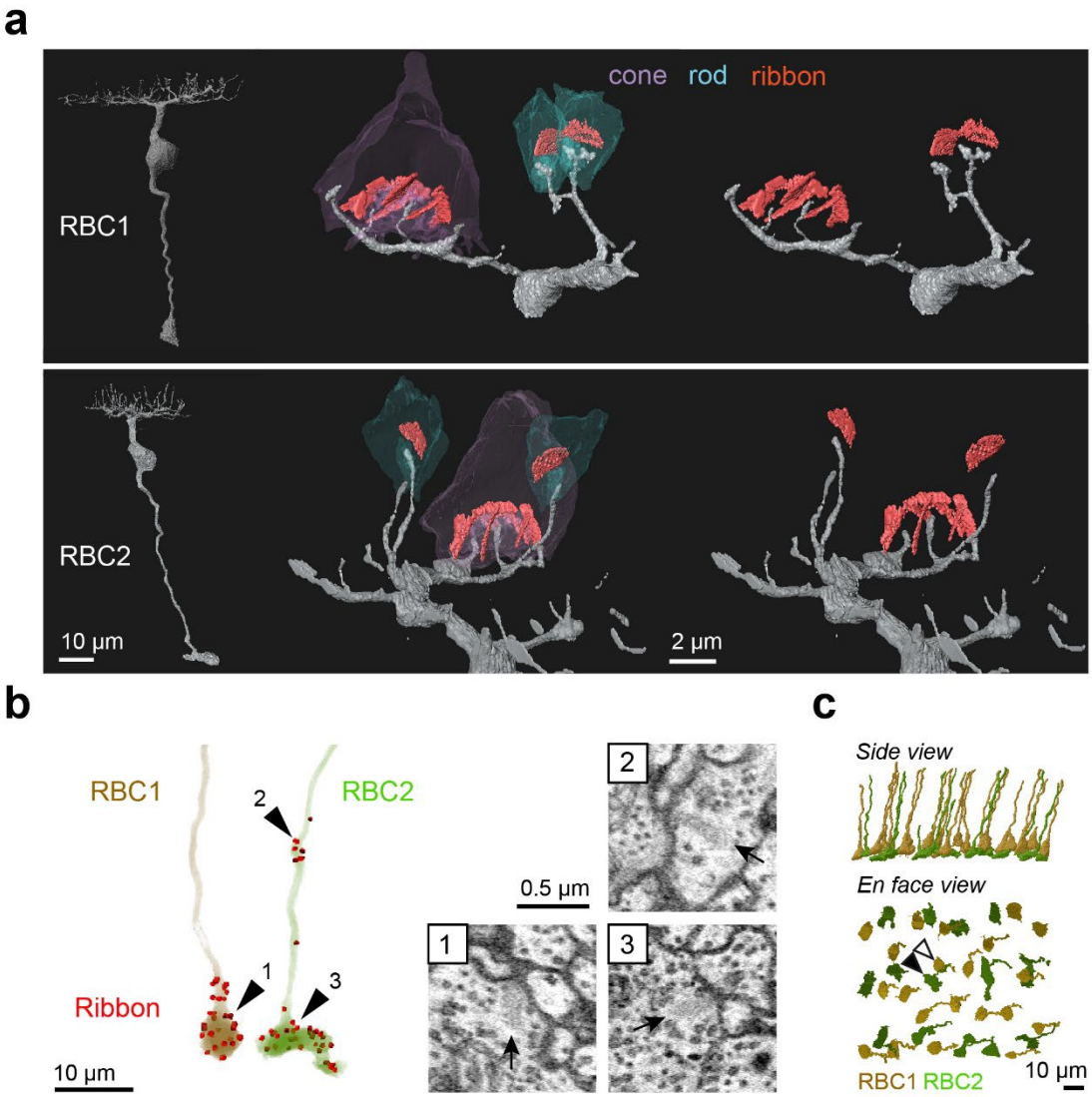

295 ***Figure 5. Identification of RBC1 and RBC2 in a SBFSEM volume.***

296 ***a**, Reconstructions of a RBC1 and a RBC2, and zoomed-in images of their dendritic tips at rod*
297 *and cone terminals. Ribbons in the rod and cones are painted red.* ***b**, Ribbon synapse distributions*
298 *in a RBC1 and a RBC2. The locations of ribbon synapses are marked in red. Arrow heads indicate*
299 *the locations of example ribbon synapses (arrows) shown in the insets.* ***c**, Reconstruction of all*
300 *RBC1s and RBC2s in the EM volume. Postsynaptic neurons of a centrally located RBC1 (open*
301 *arrow head) and RBC2 (closed arrow head) were reconstructed in Fig. 6, 7, and S5-9.*

302

303 We then focused on one RBC1 and one RBC2 in the central area of the volume and traced all of
304 their post-synaptic neuronal processes (Fig. S3c,d). Amacrine cells (ACs), unlike reginal ganglion
305 cells (RGCs), make output synapses within the retina. Hence, we identified the neuronal class
306 (e.g. AC) or RGC) for the majority (28/32) of the RBC1 postsynaptic processes and over the half
307 (18/31) of the RBC2 postsynaptic processes based on the presence or absence of presynaptic
308 structures. We found that both RBC1 and RBC2 predominantly synapse onto ACs (Fig. 6a,f). The
309 majority of the postsynaptic processes received 4 or fewer ribbon synapses from one RBC1 or
310 RBC2, with an exception of one process, which received 14 inputs from one RBC1 (Fig. 6b,g).

Figure S3

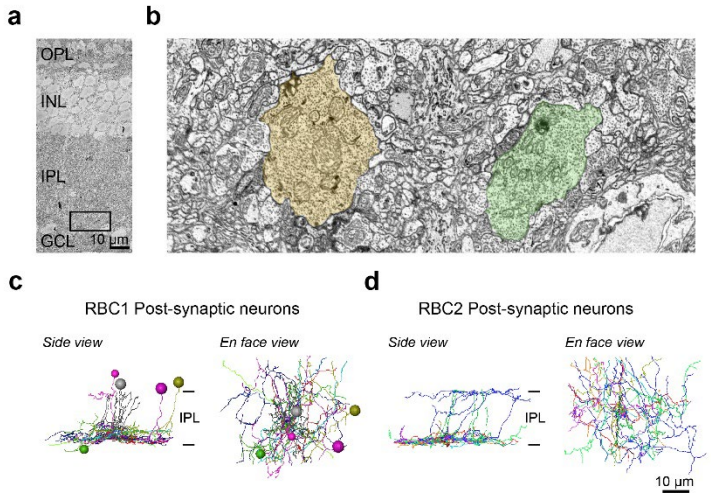

Figure S3. Identification of RBC1 and RBC2 postsynaptic neurons in SBFSEM volume

***a**, A partial image of an example SEM image of an adult zebrafish retina. OPL (outer plexiform layer), INL (inner nuclear layer), IPL (inner plexiform layer), GCL (ganglion cell*

319 *layer).* ***b****, Magnified image of the region within the black box in* ***a*** *at the bottom layer of the IPL.*
320 *Characteristic large bipolar cell axons are painted in light yellow and green.* ***c,d,*** *Traces of*
321 *neuronal processes and the location of somas of cells that are post-synaptic to RBC1 and RBC2*
322 *cells. Individual cells were color coded. IPL: inner plexiform layer.*

323

324 We further morphologically classified the postsynaptic ACs that we traced, comprising 14 cells for
325 RBC1 (Fig. S5-7) and 10 cells for RBC2 (Fig. S8,9), respectively. Most ACs extended their
326 dendrites within a single sublamina in the IPL (Fig. 6c,h). Among these mono-stratifying ACs for
327 RBC1, we identified two groups based on their dendritic stratification depth within the IPL (Fig.
328 6d,e). These two groups of ACs differed in their synaptic arrangement. ACs stratifying in the lower
329 layer formed reciprocal synapses (RS) – a synaptic arrangement that includes both input and
330 output synapses with a BC axon - with RBC1, whereas ACs stratifying in the upper layer did not
331 (Fig. 6d,e, Fig. S5,6). For RBC2, all but one AC (1/8) formed local reciprocal synapses (Fig. 6i,
332 Fig. S8,9). In addition, RBC1 formed an exceptionally high number of ribbon connections with one
333 bi-stratifying AC (marked in red in Fig. 6b,c, morphology in Fig. 7d,e and Fig. S7). In contrast,
334 RBC2 does not have a post-synaptic partner with extensive synapses.

335 Taken together, these results demonstrated that RBC1 allocated the majority (91%) of synaptic
336 outputs to 3 types of AC: 14% to non-RS ACs, 37% to RS ACs, and 40% to one bi-stratifying ACs.
337 In contrast, the RBC2 we reconstructed synapsed primarily onto a mono-stratifying AC type (68%).
338 Among 24 ACs that we traced throughout the volume, only 5 were shared between RBC1 and
339 RBC2 (Fig. S5-9). Therefore, the downstream circuits of these BC types are largely separate at
340 least at the AC level.

341

342

Figure 6

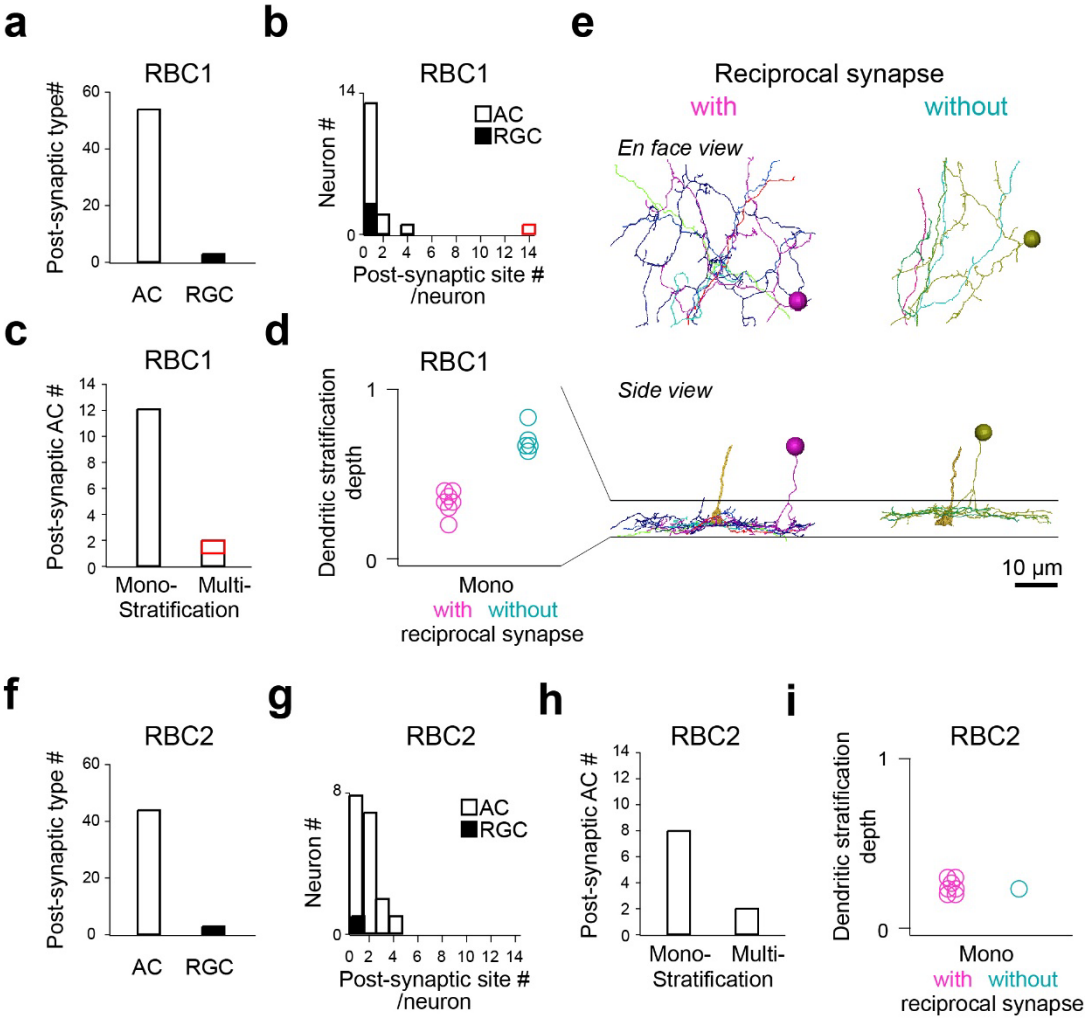

Figure 6. Identification RBC1 and RBC2 post-synaptic neuron types

***a-d**, Quantification of morphological parameters of neurons postsynaptic to one of the RBC1s in the EM volume (marked by an open arrow head in Fig. 5c). One postsynaptic neuron contained an exceptionally higher number of synapses (14) with the RBC1 (marked in red in **b** and **c**). Dendritic stratification is normalized to 0 and 1 at the lower and upper ends of the RBC1 axon terminals, respectively in **d**. **e,** Mono-stratifying ACs with (red) or without (blue) reciprocal synapses with RBC1s in the volume. The axon of the presynaptic RBC1 is also shown in the side*

view. Individual cells were color coded. ***f-i****, Quantification of morphological parameters for neurons postsynaptic to one of the RBC2s in the EM volume (marked by a closed arrow head in Fig. 5c). AC: amacrine cells, RGC: retinal ganglion cells.*

The wiring diagram of RBC1 resembles that of the mammalian primary RBC pathway

Finally, we compared the targets of RBC1 and RBC2 with those known to comprise the primary rod pathway in the mammalian retina. Mammalian RBCs synapse onto a mono-stratifed AC type called A17 and a bi-stratified AC type called A2[3,5–7]. A17 ACs are wide field ACs that synapse exclusively with RBCs and form reciprocal synapses with them[31,44], whereas A2 ACs are narrow field ACs that receive numerous (~40) synapses from RBCs but do not form reciprocal synapses with them[18,30]. Instead, A2 ACs form gap-junctions with ON CBCs through dendrites in the ON layer and output synapses onto OFF CBCs through the bouton structures in the OFF layer called lobular appendages[32].

We found that zebrafish RBC1s synapse onto both wide field ACs with reciprocal synapses (the RS ACs), resembling mammalian A17s, and a narrow field bi-stratifying ACs with extensive synaptic connections, resembling mammalian A2s (Fig. 6b-e, Fig. S5,7). By marking synaptic sites of RS ACs throughout their dendrites, we found that RS ACs are dedicated to the RBC1 pathway; synapsing predominantly (both input and output) with RBC1 and to a lesser extent with RBC2 (Fig. S5), with no synapses with other BC types (n=7 cells). This synaptic specificity and the reciprocal synapse arrangement in RS ACs mirror those of mammalian A17 ACs[31] (Fig. 7a,b).

Figure 7

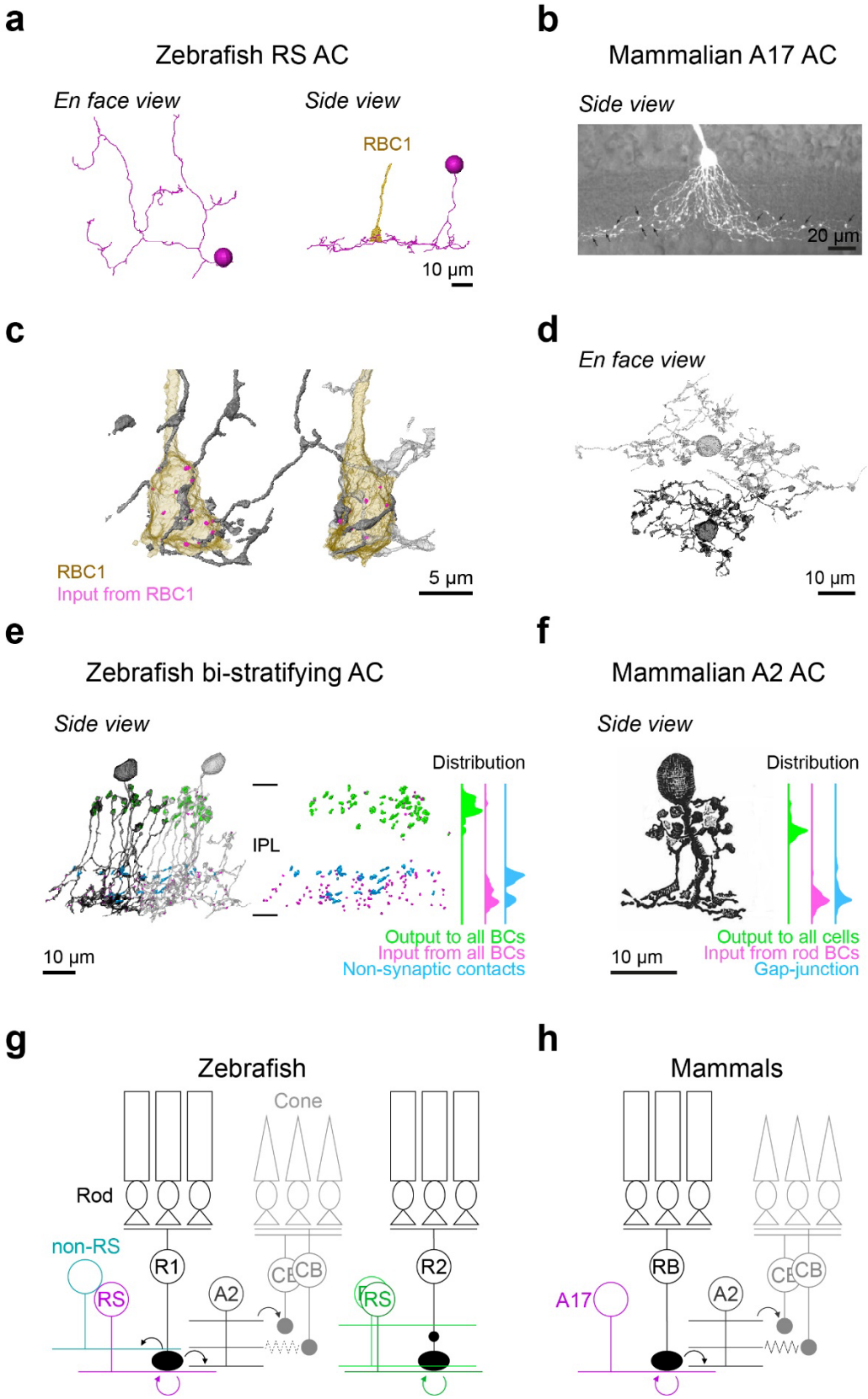
a
Zebrafish RS AC
En face view
Side view
RBC1
10 µm
b
Mammalian A17 AC
Side view
20 µm
c
RBC1
Input from RBC1
5 µm
d
En face view
10 µm
e
Zebrafish bi-stratifying AC
Side view
IPL
Distribution
10 µm
Output to all BCs
Input from all BCs
Non-synaptic contacts
f
Mammalian A2 AC
Side view
Distribution
10 µm
Output to all cells
Input from rod BCs
Gap-junction
g
Zebrafish
Cone
Rod
non-RS
RS
R1
A2
CB
R2
RS
h
Mammals
RB
A17
A2
CB

374

375 ***Figure 7. Circuit diagram of RBC1 is similar to mammalian RBC pathway***

376 ***a,*** *An example monostratified amacrine cell (RS AC) classified in Fig. 6e that formed of reciprocal*
377 *synapse with RBC1.* ***b,*** *A mouse A17 amacrine cells (taken from [47]) (**b**). **c,d,** A2-like ACs that are*
378 *postsynaptic to two neighboring RBC1s.* ***e,d****, Locations and distributions of synaptic sites and*
379 *non-synaptic contacts with BCs in zebrafish bi-stratifying AC (**e**) and in rabbit A2 ACs (taken from*
380 *[32]) (**f**). Note that synapses or non-synaptic contacts with AC and RGC are not included in (**e**), and*
381 *inputs from CBC are not included in (**f**).* ***g,h,*** *Schematic diagrams of zebrafish (**g**) and mammalian*
382 *(**h**) RBC pathways. Mouse A17 and rabbit A2 images are from [47] and [32], respectively, used with*
383 *permissions. Data for the distributions of synaptic sites within mammalian A2 ACs across the*
384 *inner plexiform layer (IPL) are taken from[48].*

385

Figure S4

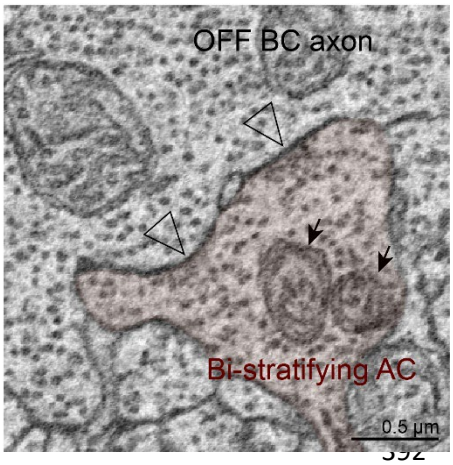

392

Figure S4. Ultrastructure of the zebrafish A2 AC boutons in the OFF layer

Examples of large synaptic sites (arrowheads) between bi-stratifying A2-like AC and OFF BC axon terminals in the OFF layer. The A2 AC boutons often contain mitochondria (arrows).

393 Next, we examined the synaptic arrangements of RBC1 with the A2-like ACs. First, we confirmed
394 that this type of AC is common to other RBC1s. By tracing the postsynaptic processes of
395 neighboring RBC1, we found another A2-like AC, which received a high number of ribbon inputs
396 from the neighboring RBC1 (Fig. 7c,d). We marked the locations of synapses with all BCs for
397 those two ACs (Fig. 7e). Gap-junctions are too small to be resolved in our SBFSEM images, but
398 as a proxy, we marked non-synaptic contacts (Fig. 7e). These revealed a striking similarity in the

399 distribution patterns of synapses and (potential) gap-junction sites across the IPL layers between
400 this AC type in zebrafish and mammalian A2 ACs (Fig. 7e,f), including the bouton structures in
401 the OFF layer that contain large presynaptic sites and mitchondria[45–47] (Fig. S4). Taken together,
402 we conclude that the circuit diagram among mammalian RBC, A2, and A17 ACs are conserved
403 in the zebrafish RBC1 pathway (Fig. 7g,h).

404 In contrast to the targets of RBC1, RBC2 formed synapses exclusively with wide-field ACs (Fig.
405 S8,9) and lack a synaptic partner with extensive synapses. Thus, RBC2 participates in a circuit
406 that differs from that of mammalian RBCs.

407

408 **DISCUSSION**

409 By combining scRNA-seq, electrophysiology, and light and electron microscopy circuit
410 reconstructions, we demonstrated that RBC1 shares many features with the mammalian primary
411 rod pathway (Fig. 7g,h), implying that the conserved rod pathway is evolutionarily ancient.

412 **The number of BC types**

413 In this study, we found 23 molecular types in adult zebrafish BCs. However, a previous
414 morphological characterization of zebrafish BCs, based on their dendritic connectivity with
415 photoreceptors and axon stratifications, identified 32 anatomical types[48]. The discrepancy in the
416 number of BC types between morphological and transcriptional characterizations may arise from
417 the regional specializations that have been documented in the larval zebrafish retina[49–52]. In any
418 event, it is clear that the adult zebrafish retina contains at least 23 BC types.

419 This number of molecular types of bipolar cells (BCs) in zebrafish, as identified in this study, is
420 higher than that found in mammals investigated to date (14-15 across mammals)[26,27,29,53], but
421 similar to that found in chick retina (22 molecular and 15 morphological BC types)[54,55]. The higher

422 number of BC types in zebrafish and chicken is not surprising, given that these species have
423 higher numbers of photoreceptor types: 5 in fish and 7 in chicks, compared to >=3 in mammals[56,57].
424 We demonstrate here one source of the increase: a single type of BC carries most of the input
425 from rods in mammals, whereas zebrafish has two RBC types.

426 **The number of RBC types**

427 Previous morphological characterization of zebrafish BCs found only one BC type that connects
428 rods and red cones. Axons of these BCs terminate in the innermost layer of the IPL[48]. We
429 speculate that this type actually includes both RBC1 and RBC2, which were combined owing to
430 their striking morphological similarity (Fig. 2,3). Consistent with this hypothesis, studies in goldfish
431 have reported two morphologically distinct "mixed" BC types that receive dominant inputs from
432 rods[22]. They have large axon terminals at the bottom of the IPL, but the axon of one mixed BC
433 type contains a smaller axonal distal bouton in the OFF layer, similar to RBC2[58]. Immunostaining
434 for PKC only labels mixed BCs without an axonal distal bouton, similar to RBC1[59]. The presence
435 of these features in goldfish suggests that RBC1 and RBC2 are conserved among teleost fish.

436 A2- and A17-like ACs may also be conserved in goldfish. Paired elecrophysiological recordings
437 between goldfish RBC1 and ACs revealed that RBC1 provides synaptic inputs to two
438 morphological types of ACs: wide-field mono-stratifying and narrow field bi-stratifying AC types[60].
439 The dendrites of the bi-stratifying ACs wrap around the RBC1 axon terminals[60], similar to A2 ACs
440 in zebrafish and mammals (Fig. 7c). Goldfish RBC1 receives GABAergic reciprocal feedback at
441 the axon terminals, like mammalian RBC[61,62]. Taken together, although it remains unknown
442 whether these two AC types in goldfish exhibit similar synaptic connectivity patterns to those of
443 mammalian A2 and A17 ACs, the findings in goldfish are consistent with the idea that the primary
444 rod pathway, including A2 and A17 ACs, is conserved in goldfish. Some differences in
445 physiological properties between mammalian RBC and goldfish RBC1 were also found. First,
446 goldfish RBC1 receives GABAergic lateral inhibition[61]. The exact cell types that provide this

447 inhibitions are unclear, but it is likely coming from the wide-field mono-stratifying ACs, as their
448 dendrites extend laterally. In contrast, mammalian A17 ACs do not provide lateral inhibition onto
449 RBCs, as each varicosity of A17 ACs at the RBC axon terminals operates independently of each
450 other[63]. Second, goldfish RBC1 exhibits spikes[64,65], whereas the spikes are only found in cone
451 BCs in mammals. Nonetheless, the absolute visual sensitivity of goldfish is comparable to that of
452 mammals[66], suggesting that the primary rod pathway we discovered in teleosts is capable of
453 transmitting information evoked by a single photon.

454 Much less is known about RBCs in other non-mammalian vertebrate species. In salamander, one
455 type of mixed ON BCs exhibit sensitivity close to that of rods[14,67]. They terminate their axons at
456 the bottom of the IPL, similar to teleosts and mammals, but it is unknown whether they express
457 the RBC marker PKC. Furthermore, the anatomical connections of BCs with rods are not yet
458 comprehensively studied in salamander. In birds, PKC labels some ON layer stratifying BC types
459 strongly[68,69]. Single-cell RNA-sequencing of chick BCs revealed a BC type that is
460 transcriptomically similar to the mammalian RBCs[55]. However, the physiological properties and
461 connections of these BCs are unknown. Moreover, a connectomic survey of chick BC types failed
462 to identify BC cells that connect with all rods in their dendritic field[54]. Unlike the species mentioned
463 above, the presumed rod bipolar cells, which have light sensitivity close to that of rods, in sea
464 lamprey are OFF type[70]. However, their connectivity with rods is unknown. Thus, it remains
465 unclear whether RBC2 orthologs are present in species other than zebrafish.

466 In mammals, morphological, molecular, and functional studies have identified only a single RBC
467 type[23,26,27,71]. Therefore, we speculate that either RBC2 evolved after the divergence between
468 teleost fish and mammals, or mammals lost this pathway.

469 **Roles of cone inputs in RBCs**

470 Cone inputs onto rod-dominant mixed BCs have been proposed to broaden the dynamic range of
471 light intensities to which they can respond[72]. Consistent with this idea, we found that both RBC1
472 and RBC2 are selective for red cones, which, with their broad spectral sensitivity, are suited for
473 encoding achromatic luminance information[73]. Because rods evolved from cones[1], we speculate
474 that RBCs may have emerged from red-cone specific CBCs. The red cone selectivity is also
475 conserved in at least one of the mixed rod dominant BC types in goldfish[74]. Although cone
476 selectivity is unknown in Salamander rod-driven mixed BCs, their spectral sensitivity curve is
477 broader at longer wavelengths than that of rods, indicating that they may connect to red cones[14].

478 Electrophysiological recording from rod-driven BCs in *Giant Danio*, a teleost fish species, showed
479 that rod and cone inputs onto rod-dominant BCs are mediated by different mechanisms: rod inputs
480 through mGluR6, whereas cone inputs through both mGluR6 and EAAT (excitatory amino acid
481 transporter)[72]. In this BC type, mGluR6 and EAAT-mediated inputs suppress each other, likely to
482 allow this cell to respond to both rod and cone dynamic ranges[72]. Electrophysiological recordings
483 in zebrafish found that some of ON BCs responded to glutamate via both mGluR6 and a
484 glutamate-gated chloride conductance increase mechanism, which is likely through EAATs[75].
485 However, the nature of EAAT contributions for cone responses in RBC1 and RBC2 is unknown.

486 While the study in *Giant Danio* suggest that mixed inputs expand the dynamic range of rod-
487 dominant BCs, electrophysiological recordings in goldfish and salamander have found that the
488 dynamic range of rod dominant BCs is similar to that of rods and that cone contributions to the
489 light response are small[14,76]. Therefore, the roles of red-cone inputs to RBCs remain to be
490 determined.

491 **Unifying mixed BCs and RBCs**

492 In mammals, it was initially thought that RBCs exclusively synapse with rods[77]. However, several
493 recent studies have demonstrated convincingly that RBCs also receive synapses from cones, at

494 least in mice and rabbits[8,77,78]. Indeed, mouse RBCs contact the majority of M-cones (~80%),
495 which are analog of zebrafish red-cone, in their dendritic territories[8]. RBCs were likely thought to
496 be exclusive to rods because of the high ratio of rods to cones in the outer nuclear layer in mice
497 and rabbits[79,80]. As a consequence, only a few cones, generally three or fewer, synapse on a
498 mouse RBC, compared to inputs from ~35 rods[8,78].

499 The rod-driven BCs in non-mammals are classically called "mixed" BCs because they connect
500 with both rods and cones. However, as argued above, this mixed connectivity is conserved in the
501 mammalian RBCs. Moreover, the dendritic specificity and connectivity of RBCs are conserved in
502 mice and zebrafish. In both species, RBCs connect with all rods and the majority of red-cones (or
503 M-cones) in their dendritic fields (Fig. 3f,h). Therefore, although the coverage of cones in mice is
504 still lower than that in zebrafish, converging rod and red-cone inputs is likely a conserved feature
505 of RBCs in all vertebrates even if the proportion and number of cone inputs may vary across
506 species. This leads us to propose that the non-mammalian mixed BCs and the mammalian RBCs
507 represent a single class of neurons, RBCs. Finally, taken together with the striking similarity in
508 the downstream circuitry of RBCs between zebrafish and mammals, we conclude that zebrafish
509 RBC1 is transcriptomically, anatomically, and functionally equivalent of mammalian RBC and that
510 they share the same evolutionary origin.

511

512 **ACKNOWLEDGEMENTS**

513 We thank the Vision Core at the University of Washington for processing zebrafish retina samples
514 and acquiring serial images for SBF-SEM. We thank Rachael N. Swanstrom for helping with cell
515 tracing of the EM volume. Funding was provided by the MCSA fellowship ("ColourFish" 748716)
516 from the EU Horizon 2020 to TY, the NIH EY14358 to ROW, U01MH105960 and R01 EY022073
517 to JRS, EY01730 (Vision Core grant, P.I. M. Neitz) Developmental Biology Training Grant

HD07183 to FDD, The Wellcome Trust 220277/Z20/Z to TB, European Research Council ERC-StG 677687 to TB, UKRI BBSRC, BB/R014817/1 and BB/W013509/1 to TB, Leverhulme Trust PLP-2017-005; RPG-2021-026 to TB, NIH grant R00EY028625 to KS, Hellmann Foundation Fellowship to KS, travel grant from Graduate School in Systemic Neuroscience to YK, and Max Planck Society to YK and HB.

AUTHOR CONTRIBUTIONS

TY, ROW, AMH, PM, JH, and YK designed the study, with input from KS, JRS, HB, and TB. YK performed single-cell RNA-seq, under the supervision of HB and JRS with guidance from KS. JH processed and analyzed the data with guidance from KS; TY and SCS generated new plasmids; TY and FDD generated novel lines; TY performed experiments, collected and analyzed the data for light microscopy with help from OL; PM performed whole-cell patch recordings; FDD prepared the sample for SBF-SEM; AMH, OL, and TY traced the EM images; TY analyzed the EM data; TY wrote the manuscript with inputs from all authors.

DECLARATION OF INTERESTS

The authors declare no competing interests.

MATERIALS AND METHODS

Animals

All procedures were performed in accordance with the University of Washington Institutional Animal Care and Use Committee guidelines, the Harvard University/Faculty of Arts & Sciences

540 Standing Committee on the Use of Animals in Research and Teaching (IACUC), and the UK
541 Animals (Scientific Procedures) act 1986 and approved by the animal welfare committee of the
542 University of Sussex. For all experiments, we used adult zebrafish (age 6-18 months) of either
543 sex that were kept at 28°C in a room with a normal 14/10 light cycles.

544 The following previously published transgenic lines were used: *Tg(vsx1:GFP)*^{nns5} [83],
545 *Tg(vsx1:memCerulean)*^{q19} [84], Tg(*trb2:tdtomato)*^{q22} [85]. In the larva *Tg(vsx1:memCerulean)*^{q19} labels
546 a subpopulation of OFF layer stratifying BCs[84]. In adults, while OFF stratifying BCs are still weakly
547 labeled, Cerulean is now strongly expressed in RBC1 (Fig. 2a,c). In addition,
548 *Tg(vsx2:memCerulean)*^{wst01} line was generated by injecting pBH-vsx2-memCerulean-pA plasmid
549 into single-cell stage eggs. Plasmid was diluted in 1x Danieau's solution to a concentration of 50
550 ng/ml. Plasmid solution was loaded into a pulled-glass micropipette, mounted to a
551 micromanipulator (Narishige), and pressure-injected via attachment to a Picospritzer II (Parker).
552 Injections were made at 10 psi for durations from 100 to 200 ms. Injected fish were raised and
553 out-crossed with wild-type fish to screen for founders. Positive progenies were raised to establish
554 transgenic lines.

555 **BC single cell RNA sequencing**

556 *BC purification and sequencing*

557 Adult zebrafish carrying the *Tg(vsx1:GFP)nns5* transgene were used to isolate BCs for single-cell
558 RNA sequencing. Retinas were dissected and digested in papain solution containing 20U/ml
559 papain, 80U/ml DNaseI, and 1.5mM L-cysteine in oxygenated (ox) Ames solution at 28°C for 45
560 minutes. The digestion was stopped by replacing the papain solution with a papain inhibitor
561 solution containing 15mg/ml ovomucoid and 15mg/ml BSA. The tissue was gently dissociated by
562 trituration using a flamed glass pipette and washed with ox. Ames containing 0.4% BSA. The
563 resulting cell suspension was filtered through a 30µm strainer and fluorescence-activated cell

564 sorting (FACS) was performed. Non-transgenic wild-type retinas were used to determine
565 background fluorescence levels and adjust sorting gates. Live bipolar cells were distinguished
566 using Calcein blue. Cells were washed, resuspended in PBS 0.04% BSA, and loaded onto the
567 microfluidic device within ~45 minutes after FACS enrichment. Droplet RNA sequencing
568 experiments were conducted on the 10X chromium platform according to the manufacturer's
569 instructions with no modifications. Up to sixteen retinas from up to eight fish per batch were
570 dissected and dissociated. Eight cDNA libraries were generated across four experiments with two
571 replicates each. The cDNA libraries were sequenced on an Illumina HiSeq 2500 to a depth of
572 ~30,000 reads per cell.

573 *Single cell transcriptomics data analysis*

574 We performed the initial preprocessing using the cellranger software suite (version 2.1.0, 10X
575 Genomics), following steps described previously in our study of Zebrafish RGCs[86]. The
576 sequencing reads were demultiplexed using "cellranger mkfastq" to obtain a separate set of
577 fastq.gz files for each of 8 samples, which were distributed across Y biological replicates. Reads
578 for each sample were aligned to the zebrafish reference transcriptome (ENSEMBL zv10, release
579 82) using "cellranger count" with default parameters to obtain a binary alignment file and a filtered
580 gene expression matrix (GEM) for each sample. To account for intronic reads, the binary
581 alignment files were processed using velocyto with default parameters[87], producing a loom file
582 containing a GEM for exonic reads and a separate matrix for intronic reads. The matrices were
583 combined for each sample, resulting in a total gene expression matrix (GEM; genes x cells)
584 summarizing transcript counts. We used the Seurat R package (Stuart et al., 2019) to combine
585 the GEMs from different channels and analyzed them for each of the biological replicates, unless
586 otherwise stated, with default parameter values. Additionally, we evaluated the robustness of our
587 clustering results to variations in select parameters. The full details of our analyses are

588 documented in markdown scripts, which are available at
589 https://github.com/shekharlab/ZebrafishBC.

590 *Preprocessing and batch integration*

591 The combined GEM was filtered to remove genes expressed in fewer than 25 cells, and cells
592 expressing fewer than 50 genes resulting in 25,233 genes and 19,492 cells. Briefly, each cell was
593 normalized to a total library size of 10,000 and the normalized counts were log-transformed using
594 the function Seurat::NormalizeData. We used Seurat::FindVariableFetures with option
595 selection.method = "vst" to identify the top 2000 highly variable genes (HVGs)[88] in each batch.
596 Next, we performed scRNA-seq integration. We used Seurat::FindIntegrationAnchors and
597 Seurat::IntegrateData, both with options "dims=1:40" to perform Canonical Correlation Analysis
598 (CCA)-based batch correction on the reduced expression matrix consisting of the HVGs. The
599 "integrated" expression values were combined across replicates, and used for dimensionality
600 reduction and clustering.

601 *Dimensionality Reduction, Clustering and Visualization*

602 To remove scale disparities between genes arising from differences in average expression levels,
603 the integrated expression values for each HVG were z-scored across the cells using
604 Seurat::ScaleData. Next, we performed Principal Component Analysis (PCA) on the scaled matrix,
605 and used Seurat::ElbowPlot to select principal components (PCs). Using the top 20 PCs, we built
606 a k-nearest neighbor graph using Seurat::FindNeighbors and identified transcriptionally distinct
607 clusters using Seurat::FindClusters, using a resolution parameter of 0.5.

608 Using the top 20 PCs, we also embedded the cells onto a 2D embedding using Uniform Manifold
609 Approximation (Becht et al., 2019) using the Seurat function RunUMAP.

610 *Identification of BCs and filtering contaminant classes*

611 BC clusters were identified based on expression of the pan-BC markers *vsx1*, and other cell
612 classes were filtered based on well known gene markers Examples of such genes include *rlbp1a*
613 and *apoeb* for Muller glia[89], *rbpms2b* for retinal ganglion cells[90], *gad1* and *gad2* for amacrine
614 cells[91], *pde6* for photoreceptors[92], and *cldn19* for endothelial cells[93]. A total of 155 cells
615 corresponding to these cell classes were removed.

616 *Hierarchical clustering*

617 To identify transcriptional relationships between BC clusters, we used
618 Seurat::FindVariableFeatures to recalculate the top 2000 most variable genes. The average
619 expression values of genes in each cluster were used as input for hierarchical clustering,
620 performed using pvclust with parameters method.hclust = "complete" and method.dist =
621 "correlation". The resulting output was visualized as a dendrogram.

622 **Plasmid construction**

623 Plasmid pBH-vsx2-memCerulean-pA was made using the Gateway system (ThermoFisher,
624 12538120) with combinations of entry and destination plasmids as follows: pTol2CG2 [94], p5E-
625 vsx2, pME-membrane-Cerulean, p3E-pA (Kwan et al., 2007). Plasmid p5E-vsx2 was generated
626 by inserting a polymerase chain reaction (PCR)-amplified vsx2 promoter genomic fragment into
627 p5E plasmid using BP clonase (ThermoFisher, 11789013). PCR reaction was performed using
628 primers: 5'-GGGGACAACTTTGTATAGAAAAGTTGATGCTAAACAACTTCAAACGACCAA-3'
629 and 5'-GGGGACTGCTTTTTTGTACAAACTTGGCCTCTGAGACTATTCCCTTCTTTG-3'.

630 **Immunostaining and light microscopy imaging**

631 Adult zebrafish were humanely euthanized in ice-chilled fish water. After decapitation, retinal
632 tissues were dissected from the enucleated whole eyes by removing cornea, lens, and epithelial
633 layer in 1x in phosphate-buffered saline (PBS). The tissue were immediately fixed in 4%
634 paraformaldehyde (Agar Scientific, AGR1026) in PBS for 20 min at room temperature (RT)

635 followed by three washes in PBS. For retinal slice preparation, the tissues were mounted in 2%
636 agarose in PBS and sliced at 100 or 200 μm thickness using vibratome (TPI 1000). For rod
637 staining, the tissues were sliced horizontally, parallel to the outer plexiform layer (OPL), to
638 facilitate antibody penetration in the tissue while preserving bipolar cell dendrites in the OPL.
639 Sliced or the whole retinal samples were treated with PBS containing 0.2% Triton X-100 (Sigma-
640 Aldrich, X100) for at least 10 min and up to 1 day, followed by the addition of primary antibodies.
641 After 3 to 5 days of incubation at 4°C, samples were washed three times with PBS and 0.2%
642 Triton X-100 solution and treated with secondary antibodies. After 1 day of incubation, samples
643 were mounted in 1% agar in PBS on a coverslip, and subsequently, PBS was replaced with
644 mounting media (VECTASHIELD, H-1000) for imaging.

645 Primary antibodies were 4C12 antibody (mouse, 1:50; kindly provided by Jim Fadool [95] and anti-
646 mGluR6b antidoby (rabbit, 1:500; kindly provided by Stephan CF Neuhauss [96]). Secondary
647 antibodies were AlexaFluor594 anti-rabbit (donkey, 1:500; Jackson ImmunoResearch
648 Laboratories 711-586-152) and DyLight647 anti-mouse (donkey, 1:500; Jackson
649 ImmunoResearch Laboratories 715-606-150). Confocal image stacks were taken on a TCS SP8
650 (Leica) with a 63× oil immersion objective (HC PL APO CS2, Leica). Typical voxel size was 90
651 nm and 0.5 μm in xy and z, respectively. Super-resolution images were taken on an OMX (General
652 Electric). Contrast, brightness, and pseudo-color were adjusted for display in Fiji [National
653 Institutes of Health (NIH)].

654 Image stacks were median filtered in Fiji. For some images, maximum-intensity projections were
655 generated in Amira (FEI). 3D image reconstructions were digitally sliced using the Amira slice
656 functions. All measurements were made in Fiji.

657 **Image Analysis**

658 *Quantitation of cell density*

659 We obtained the cell density of RBC1 and RBC2 by counting the axon terminals of these cells
660 within regions of interest from confocal image stacks of the dorsal and ventro-temporal retina.
661 RBC2 was counted from images of the *Tg(vsx2:memCerulean)*^{wst01} line. Because not all RBC1
662 labeled in the *Tg(vsx1:memCerulean)*^{q19} line express mCerulean, we quantified the density of
663 PKC labeled cells with axon terminals in the bottom layer of the IPL. Counts were obtained from
664 3-4 retinas from 3 animals of each line. For RBC1, axons were quantified within an area between
665 37,000 and 85,000 μm^2, and for RBC2, the areas were between 11,000 -22,000 μm^2.

666 *Dendritic field*

667 The dendritic field was defined by tracing the extent of a given cell's dendrites with the polygonal
668 select tool, and removing any concavity using FIJI (see Figure S2). The dendritic arbor area was
669 then obtained by calculating the area enclosed by the polygon. Because the dendritic tips of some
670 neighboring cells of the same type overlapped and could not be distinguished readily, one
671 investigator repeatedly traced (3 to 4 measurements for a single cell) the dendrite boundary, and
672 obtained the respective area for a given cell until at least three measurements were within ± 2.5%
673 of the average of all previous measurements for that cell. Confocal images from three fish were
674 used, with images of RBC1 and RBC2 cells acquired from the dorsal and ventral regions of the
675 retina: 10 to 17 cells per fish were measured for each location and cell type, resulting in a total of
676 33 to 41 cells measured for each location and cell type.

677 *Photoreceptor connectivity*

678 Dendritic contacts with photoreceptors were defined by the co-localization of dendritic tips
679 extending towards outer nucleus layer and photoreceptor terminals by scrolling through confocal
680 image stack in Fiji. The percentage contacted was computed by dividing the number of
681 photoreceptors contacted by a given BC by the number of photoreceptors within the dendritic field
682 of the BC.

683 **Electrophysiology**

684 Fish (3-6 months old) used in physiology experiments were dark adapted for at least 2 hours, and
685 the retinas were isolated under infrared light following procedures approved by the Administrative
686 Panel on Laboratory Animal Care at the University of Washington. Retinas were continuously
687 superfused (~8 mL/min) with oxygenated (95% O2, 5% CO2) bicarbonate-buffered Ames solution
688 (Sigma) maintained at 25ºC–28ºC.

689 Recordings were conducted in a flat-mount preparation with photoreceptors facing down. Bipolar
690 cells were patched at the axon terminals. To access bipolar cell terminals for recording, small
691 groups of ganglion cells were suctioned off the top of the retina to expose the inner plexiform
692 layer. Terminals of RBC1 bipolar cells could be targeted for recording using only infrared
693 illumination, whereas RBC2 terminals, which were not easily visible without fluorescence imaging,
694 were targeted using a custom-built two-photon microscope. As a result, measuring rod-mediated
695 responses in RBC2 was unfeasible due to the compromise of rod responses by two-photon
696 imaging.

697 Whole-cell voltage-clamp recordings were obtained using patch pipettes filled with a Cs+-based
698 internal solution. This internal solution also included Alexa Fluor 594, which was used for two-
699 photon imaging of each cell after recording to confirm its type by morphology. To isolate excitatory
700 postsynaptic currents, we voltage-clamped cells near the reversal potential for chloride-mediated
701 conductances (~-60 mV). In addition, to block inhibitory synaptic transmission, we added the
702 GABAA receptor antagonist gabazine (20 μM), the GABAC receptor antagonist TPMPA (50 μM),
703 and the glycine receptor antagonist strychnine (3 μM) to the superfusion solution. In experiments
704 in which mGluR6-mediated input was blocked, the mGluR6 receptor agonist APB (10 μM) was
705 also added to the superfusion.

706 Light from blue or red light-emitting diodes (LEDs, peak output = 470 nm and 640 nm respectively)
707 was delivered to the recording chamber via fiber optic cable positioned beneath the microscope's
708 condenser lens. The light uniformly illuminated a circular area through an aperture 0.5 mm in
709 diameter centered on the recorded cell. Protocols for light stimulation were designed to either
710 activate rods only (using the blue LED) or both rods and cones (using the red LED).

711 **EM data acquisition, reconstruction, and annotation**

712 Dissected retinal tissues from wild type adult zebrafish were immediately transferred into a 1.5-
713 ml tube with the fixative (4% glutaraldehyde in 0.1M cacodylate buffer [pH7.4]) and incubated
714 overnight on a shaker at RT. Subsequently, the tissue was washed three times in 0.1 M
715 cacodylate buffer (pH7.4) and incubated in a solution containing 1.5% potassium ferrocyanide
716 and 2% osmium tetroxide (OsO4) in 0.1 M cacodylate buffer [0.66% lead in 0.03 M aspartic acid
717 (pH 5.5)] for 1 hour. After washing, the tissue was placed in a freshly made thiocarbohydrazide
718 (TCH) solution (0.1 g of TCH in 10 ml of double-distilled H2O heated to 600°C for 1 hour) for 20
719 min at RT. After another rinse, at RT, the tissue was incubated in 2% OsO4 for 30 min at RT. The
720 samples were rinsed again and stained en bloc in 1% uranyl acetate overnight at 40°C, washed,
721 and stained with Walton's lead aspartate for 30 min. After a final wash, the retinal pieces were
722 dehydrated in a graded ice-cold alcohol series and placed in propylene oxide at RT for 10 min.
723 Last, the sample was embedded in Durcupan resin. Semithin sections (0.5 to 1 μm thick) were
724 cut and stained with toluidine blue, until the fiducial marks (box) in the ganglion cell layer (GCL)
725 appeared. The block was then trimmed and mounted in a serial block-face scanning electron
726 microscope (GATAN/Zeiss, 3View). Serial sections were cut at a thickness of 70 nm and imaged
727 at an xy resolution of 7 nm. Six tiles, each about 40 μm by 40 μm with an overlap of about 10%,
728 covering from the outer nucleus layer to the ganglion cell layer in a side view was obtained. Retinal
729 location was not recorded. The image stacks were concatenated and aligned using TrakEM2
730 (NIH). Neurons were traced or painted using the tracing and painting tools in TrakEM2.

731 **Statistics**

732 Mann-Whitney U test was used to determine the *p*-value for comparing dendritic field sizes.

733

734 **DATA AVAILABILITY**

735 Computational scripts detailing scRNA-seq analysis reported in this paper are available at
736 https://github.com/shekharlab/

737 ZebrafishBC. We have also provided R markdown (Rmd) files that show step-by-step
738 reproduction of the key results at https://github.com/shekharlab/ZebrafishBC. The raw and
739 processed scRNA-seq data reported in this paper was obtained from the Gene Expression
740 Omnibus (GEO) entry GSE237215 (subseries GSE237214).

741

742

743

744

745

746

747

748

749

750

751

Figure S5

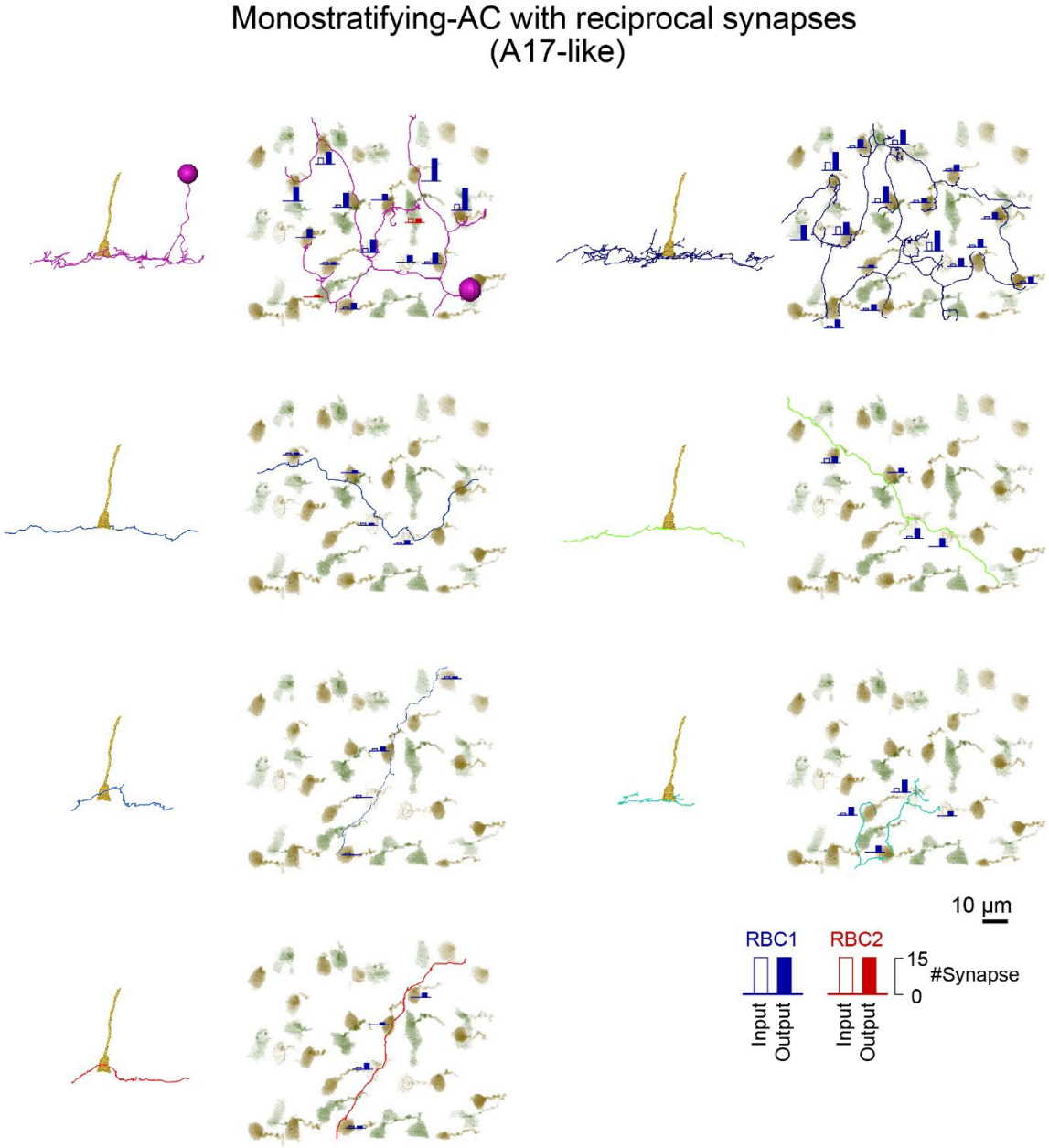

752

753 **Figure S5. Gallery of mono-stratifying AC making reciprocal synapses with RBC1**

754 *En face* and side views of individual cells or processes. The numbers of input (open bar) and
755 output (closed bar) synapses with each RBC1 (blue) and RBC2 (red) terminal are indicated as
756 the height of the bars.

Figure S6

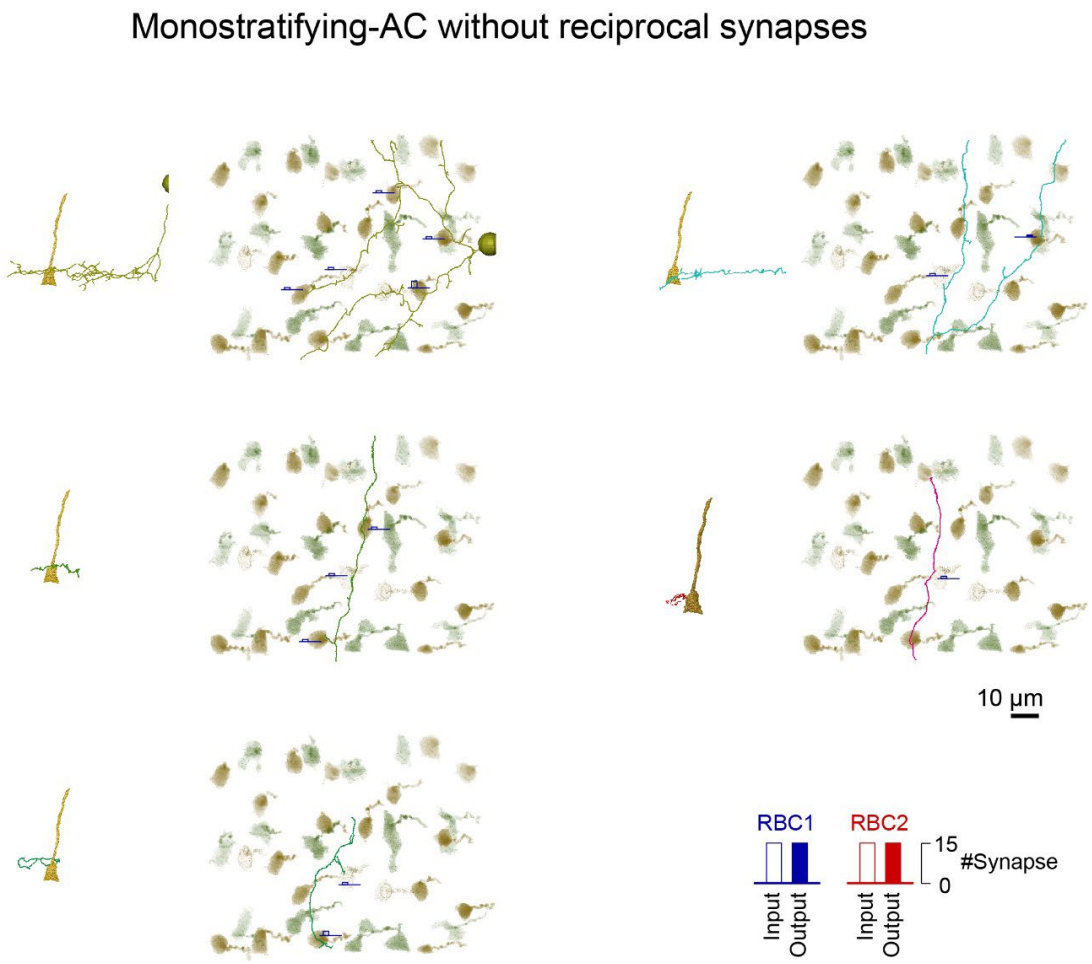

757

758 **Figure S6. Gallery of mono-stratifying AC without reciprocal synapses with RBC1**

759 *En face* and side views of individual cells. The numbers of input (open bar) and output (closed
760 bar) synapses with each RBC1 (blue) and RBC2 (red) terminal are indicated as the height of the
761 bars.

762

763

764

Figure S7

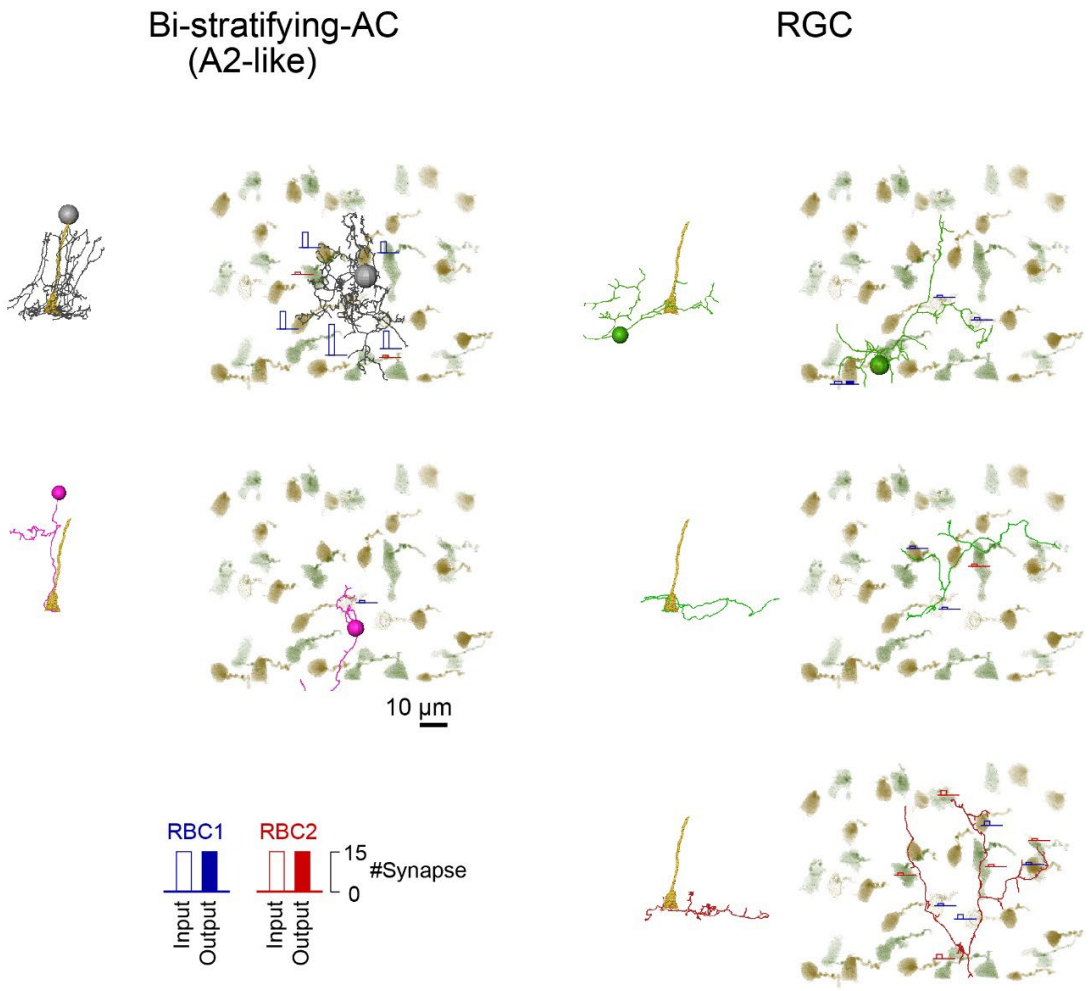

765

766 **Figure S7. Gallery of bi-stratifying AC and RGC contacted to RBC1**

767 *En face* and side views of individual cells. The numbers of input (open bar) and output (closed
768 bar) synapses with each RBC1 (blue) and RBC2 (red) terminal are indicated as the height of the
769 bars.

770

771

772

Figure S8

Monostratifying-AC with reciprocal synapses

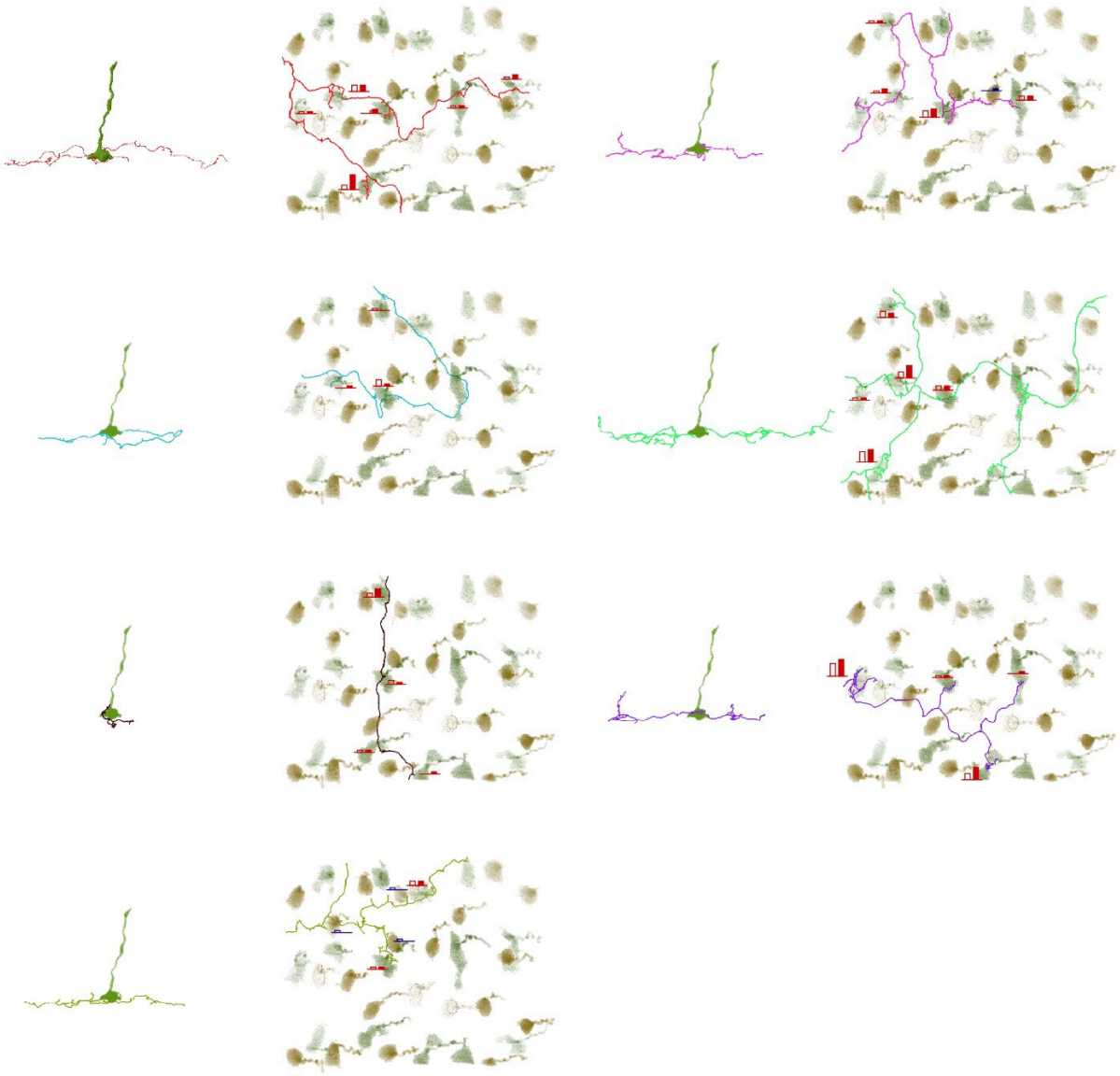

Monostratifying-AC without reciprocal synapses

773

774 **Figure S8. Gallery of mono-stratifying AC connected to RBC2**

775 *En face* and side views of individual cells. The numbers of input (open bar) and output (closed
776 bar) synapses with each RBC1 (blue) and RBC2 (red) terminal are indicated as the height of the
777 bars.

778

Figure S9

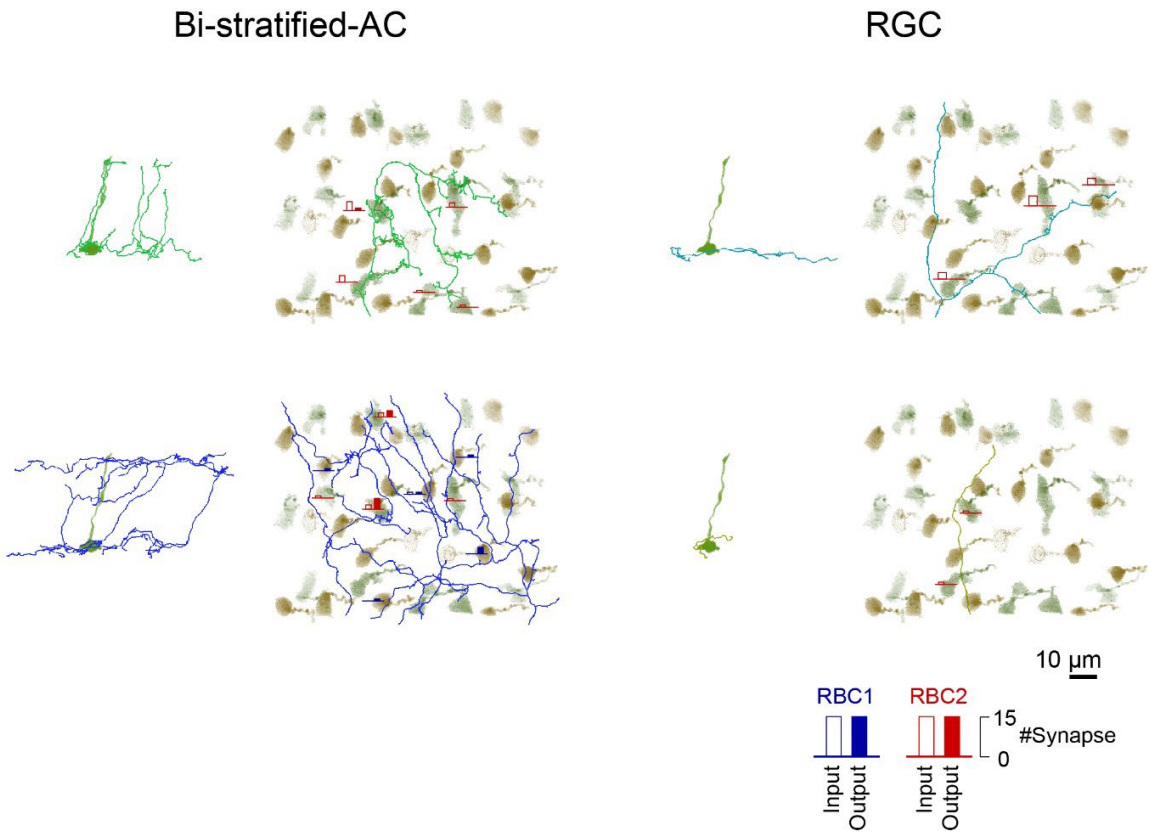

779

780 **Figure S9. Gallery of bi-stratifying AC and RGC connected to RBC2**

781 *En face* and side views of individual cells. The numbers of input (open bar) and output (closed
782 bar) synapses with each RBC1 (blue) and RBC2 (red) terminal are indicated as the height of the
783 bars.

784 **REFERENCES**

785 1. Morshedian, A. & Fain, G. L. The evolution of rod photoreceptors. *Philos. Trans. R. Soc. B Biol. Sci.*
786 **372**, 20160074 (2017).
787 2. Bloomfield, S. A. & Dacheux, R. F. Rod Vision: Pathways and Processing in the Mammalian Retina.
788 *Prog. Retin. Eye Res.* **20**, 351–384 (2001).
789 3. Field, G. D., Sampath, A. P. & Rieke, F. RETINAL PROCESSING NEAR ABSOLUTE THRESHOLD: From
790 Behavior to Mechanism. *Annu. Rev. Physiol.* **67**, 491–514 (2005).
791 4. Grimes, W. N., Songco-Aguas, A. & Rieke, F. Parallel Processing of Rod and Cone Signals: Retinal
792 Function and Human Perception. *Annu. Rev. Vis. Sci.* **4**, 123–141 (2018).
793 5. Strettoi, E. 1.11 - Mammalian Rod Pathways. in *The Senses: A Comprehensive Reference* (eds.
794 Masland, R. H. et al.) 303–311 (Academic Press, 2008). doi:10.1016/B978-012370880-9.00266-8.
795 6. Wu, S. M. Synaptic Organization of the Vertebrate Retina: General Principles and Species-Specific
796 Variations: The Friedenwald Lecture. *Invest. Ophthalmol. Vis. Sci.* **51**, 1264–1274 (2010).
797 7. Thoreson, W. B. & Dacey, D. M. Diverse Cell Types, Circuits, and Mechanisms for Color Vision in the
798 Vertebrate Retina. *Physiol. Rev.* **99**, 1527–1573 (2019).
799 8. Behrens, C., Schubert, T., Haverkamp, S., Euler, T. & Berens, P. Connectivity map of bipolar cells and
800 photoreceptors in the mouse retina. *eLife* **5**, e20041 (2016).
801 9. Baylor, D. A., Lamb, T. D. & Yau, K. W. Responses of retinal rods to single photons. *J. Physiol.* **288**,
802 613–634 (1979).
803 10. Baylor, D. A., Nunn, B. J. & Schnapf, J. L. The photocurrent, noise and spectral sensitivity of rods of
804 the monkey Macaca fascicularis. *J. Physiol.* **357**, 575–607 (1984).
805 11. Field, G. D. & Rieke, F. Nonlinear Signal Transfer from Mouse Rods to Bipolar Cells and Implications
806 for Visual Sensitivity. *Neuron* **34**, 773–785 (2002).

807 12. Field, G. D. & Rieke, F. Mechanisms regulating variability of the single photon responses of
808 mammalian rod photoreceptors. *Neuron* **35**, 733–747 (2002).
809 13. Ingram, N. T., Sampath, A. P. & Fain, G. L. Why are rods more sensitive than cones? *J. Physiol.* **594**,
810 5415–5426 (2016).
811 14. Yang, X.-L. & Wu, S. M. Response Sensitivity and Voltage Gain of the Rod- and Cone-Bipolar Cell
812 Synapses in Dark-Adapted Tiger Salamander Retina. *J. Neurophysiol.* **78**, 2662–2673 (1997).
813 15. Kolb, H. & Famiglietti, E. V. Rod and Cone Pathways in the Inner Plexiform Layer of Cat Retina.
814 *Science* **186**, 47–49 (1974).
815 16. Strettoi, E., Masri, R. A. & Grünert, U. AII amacrine cells in the primate fovea contribute to photopic
816 vision. *Sci. Rep.* **8**, 16429 (2018).
817 17. Lee, S. C. S., Martin, P. R. & Grünert, U. Topography of Neurons in the Rod Pathway of Human
818 Retina. *Invest. Ophthalmol. Vis. Sci.* **60**, 2848–2859 (2019).
819 18. Tsukamoto, Y., Morigiwa, K., Ueda, M. & Sterling, P. Microcircuits for Night Vision in Mouse Retina.
820 *J. Neurosci.* **21**, 8616–8623 (2001).
821 19. Kolb, H. & Nelson, R. Rod pathways in the retina of the cat. *Vision Res.* **23**, 301–312 (1983).
822 20. Dacheux, R. F. & Raviola, E. The rod pathway in the rabbit retina: a depolarizing bipolar and
823 amacrine cell. *J. Neurosci.* **6**, 331–345 (1986).
824 21. Freed, M. A., Smith, R. G. & Sterling, P. Rod bipolar array in the cat retina: pattern of input from rods
825 and GABA-accumulating amacrine cells. *J. Comp. Neurol.* **266**, 445–455 (1987).
826 22. Joselevitch, C. & Kamermans, M. Retinal parallel pathways: Seeing with our inner fish. *Vision Res.*
827 **49**, 943–959 (2009).
828 23. Franke, K. *et al.* Inhibition decorrelates visual feature representations in the inner retina. *Nature*
829 **542**, 439–444 (2017).

830 24. Ghosh, K. K., Bujan, S., Haverkamp, S., Feigenspan, A. & Wässle, H. Types of bipolar cells in the
831 mouse retina. *J. Comp. Neurol.* **469**, 70–82 (2004).
832 25. Grünert, U. & Martin, P. R. Cell types and cell circuits in human and non-human primate retina.
833 *Prog. Retin. Eye Res.* 100844 (2020) doi:10.1016/j.preteyeres.2020.100844.
834 26. Peng, Y.-R. *et al.* Molecular Classification and Comparative Taxonomics of Foveal and Peripheral
835 Cells in Primate Retina. *Cell* **176**, 1222-1237.e22 (2019).
836 27. Shekhar, K. *et al.* Comprehensive Classification of Retinal Bipolar Neurons by Single-Cell
837 Transcriptomics. *Cell* **166**, 1308-1323.e30 (2016).
838 28. Masland, R. H. The neuronal organization of the retina. *Neuron* **76**, 266–80 (2012).
839 29. Hahn, J. *et al.* Evolution of neuronal cell classes and types in the vertebrate retina.
840 2023.04.07.536039 Preprint at https://doi.org/10.1101/2023.04.07.536039 (2023).
841 30. Strettoi, E., Dacheux, R. F. & Raviola, E. Synaptic connections of rod bipolar cells in the inner
842 plexiform layer of the rabbit retina. *J. Comp. Neurol.* **295**, 449–466 (1990).
843 31. Zhang, C., Hellevik, A., Takeuchi, S. & Wong, R. O. Hierarchical partner selection shapes rod-cone
844 pathway specificity in the inner retina. *iScience* **25**, 105032 (2022).
845 32. Strettoi, E., Raviola, E. & Dacheux, R. F. Synaptic connections of the narrow-field, bistratified rod
846 amacrine cell (AII) in the rabbit retina. *J. Comp. Neurol.* **325**, 152–168 (1992).
847 33. Dunn, F. A. & Rieke, F. Single-Photon Absorptions Evoke Synaptic Depression in the Retina to Extend
848 the Operational Range of Rod Vision. *Neuron* **57**, 894–904 (2008).
849 34. Grimes, W. N., Hoon, M., Briggman, K. L., Wong, R. O. & Rieke, F. Cross-synaptic synchrony and
850 transmission of signal and noise across the mouse retina. *eLife* **3**, e03892 (2014).
851 35. Pang, J.-J., Gao, F. & Wu, S. M. Light-evoked current responses in rod bipolar cells, cone depolarizing
852 bipolar cells and AII amacrine cells in dark-adapted mouse retina. *J. Physiol.* **558**, 897–912 (2004).

853 36. Demb, J. B. & Singer, J. H. Intrinsic properties and functional circuitry of the AII amacrine cell. *Vis.*
854 *Neurosci.* **29**, 51–60 (2012).
855 37. Strettoi, E., Dacheux, R. F. & Raviola, E. Cone bipolar cells as interneurons in the rod, pathway of the
856 rabbit retina. *J. Comp. Neurol.* **347**, 139–149 (1994).
857 38. Vitorino, M. *et al.* Vsx2 in the zebrafish retina: restricted lineages through derepression. *Neural*
858 *Develop.* **4**, 14 (2009).
859 39. Križaj, D., Cordeiro, S. & Strauß, O. Retinal TRP channels: Cell-type-specific regulators of retinal
860 homeostasis and multimodal integration. *Prog. Retin. Eye Res.* **92**, 101114 (2023).
861 40. Wässle, H., Yamashita, M., Greferath, U., Grünert, U. & Müller, F. The rod bipolar cell of the
862 mammalian retina. *Vis. Neurosci.* **7**, 99–112 (1991).
863 41. Wässle, H., Puller, C., Müller, F. & Haverkamp, S. Cone Contacts, Mosaics, and Territories of Bipolar
864 Cells in the Mouse Retina. *J. Neurosci.* **29**, 106–117 (2009).
865 42. Vihtelic, T. S., Doro, C. J. & Hyde, D. R. Cloning and characterization of six zebrafish photoreceptor
866 opsin cDNAs and immunolocalization of their corresponding proteins. *Vis. Neurosci.* **16**, 571–585
867 (1999).
868 43. Chinen, A., Hamaoka, T., Yamada, Y. & Kawamura, S. Gene Duplication and Spectral Diversification
869 of Cone Visual Pigments of Zebrafish. *Genetics* **163**, 663–675 (2003).
870 44. Sandell, J. H., Masland, R. H., Raviola, E. & Dacheux, R. F. Connections of indoleamine-accumulating
871 cells in the rabbit retina. *J. Comp. Neurol.* **283**, 303–313 (1989).
872 45. Gamlin, C. R., Zhang, C., Dyer, M. A. & Wong, R. O. L. Distinct Developmental Mechanisms Act
873 Independently to Shape Biased Synaptic Divergence from an Inhibitory Neuron. *Curr. Biol. CB* **30**,
874 1258-1268.e2 (2020).
875 46. Marc, R. E., Anderson, J. R., Jones, B. W., Sigulinsky, C. L. & Lauritzen, J. S. The AII amacrine cell
876 connectome: a dense network hub. *Front. Neural Circuits* **8**, (2014).

877 47. Tsukamoto, Y. & Omi, N. Functional allocation of synaptic contacts in microcircuits from rods via rod
878 bipolar to AII amacrine cells in the mouse retina. *J. Comp. Neurol.* **521**, 3541–3555 (2013).
879 48. Li, Y. N., Tsujimura, T., Kawamura, S. & Dowling, J. E. Bipolar Cell-Photoreceptor Connectivity in the
880 Zebrafish (Danio rerio) Retina. *J. Comp. Neurol.* **520**, 3786–3802 (2012).
881 49. Zimmermann, M. J. Y. *et al.* Zebrafish Differentially Process Color across Visual Space to Match
882 Natural Scenes. *Curr. Biol. CB* **28**, 2018-2032.e5 (2018).
883 50. Zhou, M. *et al.* Zebrafish Retinal Ganglion Cells Asymmetrically Encode Spectral and Temporal
884 Information across Visual Space. *Curr. Biol.* **30**, 2927-2942.e7 (2020).
885 51. Yoshimatsu, T., Schröder, C., Nevala, N. E., Berens, P. & Baden, T. Fovea-like Photoreceptor
886 Specializations Underlie Single UV Cone Driven Prey-Capture Behavior in Zebrafish. *Neuron* **107**,
887 320-337.e6 (2020).
888 52. Schröder, C., Oesterle, J., Berens, P., Yoshimatsu, T. & Baden, T. Distinct synaptic transfer functions
889 in same-type photoreceptors. *eLife* **10**, e67851 (2021).
890 53. Yan, W. *et al.* Cell Atlas of The Human Fovea and Peripheral Retina. *Sci. Rep.* **10**, 9802 (2020).
891 54. Günther, A. *et al.* Double Cones and the Diverse Connectivity of Photoreceptors and Bipolar Cells in
892 an Avian Retina. *J. Neurosci.* **41**, 5015–5028 (2021).
893 55. Yamagata, M., Yan, W. & Sanes, J. R. A cell atlas of the chick retina based on single-cell
894 transcriptomics. *eLife* **10**, e63907 (2021).
895 56. Baden, T. & Osorio, D. The Retinal Basis of Vertebrate Color Vision. *Annu. Rev. Vis. Sci.* **5**, 177–200
896 (2019).
897 57. Lamb, T. D. Evolution of phototransduction, vertebrate photoreceptors and retina. *Prog. Retin. Eye*
898 *Res.* **36**, 52–119 (2013).
899 58. Sherry, D. M. & Yazulla, S. Goldfish bipolar cells and axon terminal patterns: A Golgi study. *J. Comp.*
900 *Neurol.* **329**, 188–200 (1993).

901 59. Behrens, U. D., Borde, J., Mack, A. F. & Wagner, H.-J. Distribution of phosphorylated protein kinase C
902 alpha in goldfish retinal bipolar synaptic terminals: control by state of adaptation and
903 pharmacological treatment. *Cell Tissue Res.* **327**, 209–220 (2007).
904 60. Kim, M.-H. & von Gersdorff, H. Postsynaptic Plasticity Triggered by Ca2+-Permeable AMPA Receptor
905 Activation in Retinal Amacrine Cells. *Neuron* **89**, 507–520 (2016).
906 61. Vigh, J., Vickers, E. & von Gersdorff, H. Light-evoked lateral GABAergic inhibition at single bipolar cell
907 synaptic terminals is driven by distinct retinal microcircuits. *J. Neurosci. Off. J. Soc. Neurosci.* **31**,
908 15884–15893 (2011).
909 62. Vigh, J. & Gersdorff, H. von. Prolonged Reciprocal Signaling via NMDA and GABA Receptors at a
910 Retinal Ribbon Synapse. *J. Neurosci.* **25**, 11412–11423 (2005).
911 63. Grimes, W. N., Zhang, J., Graydon, C. W., Kachar, B. & Diamond, J. S. Retinal parallel processors:
912 more than 100 independent microcircuits operate within a single interneuron. *Neuron* **65**, 873–885
913 (2010).
914 64. Burrone, J. & Lagnado, L. Electrical resonance and Ca2+ influx in the synaptic terminal of
915 depolarizing bipolar cells from the Goldfish retina. *J. Physiol.* **505**, 571–584 (1997).
916 65. Protti, D. A., Flores-Herr, N. & von Gersdorff, H. Light Evokes Ca2+ Spikes in the Axon Terminal of a
917 Retinal Bipolar Cell. *Neuron* **25**, 215–227 (2000).
918 66. Powers, M. K. & Easter, S. S. Absolute visual sensitivity of the goldfish. *Vision Res.* **18**, 1137–1147
919 (1978).
920 67. Pang, J.-J., Gao, F. & Wu, S. M. Stratum-by-stratum projection of light response attributes by retinal
921 bipolar cells of Ambystoma. *J. Physiol.* **558**, 249–262 (2004).
922 68. Balaji, V. *et al.* Immunohistochemical characterization of bipolar cells in four distantly related avian
923 species. *J. Comp. Neurol.* **531**, 561–581 (2023).

924 69. Caminos, E., Velasco, A., Jarrín, M., Aijón, J. & Lara, J. M. Protein kinase C-like immunoreactive cells
925 in embryo and adult chicken retinas. *Dev. Brain Res.* **118**, 227–230 (1999).
926 70. Frederiksen, R., Fain, G. L. & Sampath, A. P. A hyperpolarizing rod bipolar cell in the sea lamprey,
927 Petromyzon marinus. *J. Exp. Biol.* **225**, jeb243949 (2022).
928 71. Tsukamoto, Y. & Omi, N. Classification of Mouse Retinal Bipolar Cells: Type-Specific Connectivity
929 with Special Reference to Rod-Driven AII Amacrine Pathways. *Front. Neuroanat.* **11**, 92 (2017).
930 72. Wong, K. Y., Cohen, E. D. & Dowling, J. E. Retinal Bipolar Cell Input Mechanisms in Giant Danio. II.
931 Patch-Clamp Analysis of on Bipolar Cells. *J. Neurophysiol.* **93**, 94–107 (2005).
932 73. Yoshimatsu, T. *et al.* Ancestral circuits for vertebrate color vision emerge at the first retinal synapse.
933 *Sci. Adv.* **7**, eabj6815 (2021).
934 74. Ishida, A. T., Stell, W. K. & Lightfoot, D. O. Rod and cone inputs to bipolar cells in goldfish retina. *J.*
935 *Comp. Neurol.* **191**, 315–335 (1980).
936 75. Connaughton, V. P. & Nelson, R. Axonal stratification patterns and glutamate-gated conductance
937 mechanisms in zebrafish retinal bipolar cells. *J. Physiol.* **524 Pt 1**, 135–46 (2000).
938 76. Joselevitch, C. & Kamermans, M. Interaction between rod and cone inputs in mixed-input bipolar
939 cells in goldfish retina. *J. Neurosci. Res.* **85**, 1579–1591 (2007).
940 77. Pang, J.-J. *et al.* Direct rod input to cone BCs and direct cone input to rod BCs challenge the
941 traditional view of mammalian BC circuitry. *Proc. Natl. Acad. Sci.* **107**, 395–400 (2010).
942 78. Whitaker, C. M., Nobles, G., Ishibashi, M. & Massey, S. C. Rod and Cone Connections With Bipolar
943 Cells in the Rabbit Retina. *Front. Cell. Neurosci.* **15**, 662329 (2021).
944 79. Carter-Dawson, L. D. & LaVail, M. M. Rods and cones in the mouse retina. I. Structural analysis using
945 light and electron microscopy. *J. Comp. Neurol.* **188**, 245–262 (1979).

946 80. Famiglietti, E. V. & Sharpe, S. J. Regional topography of rod and immunocytochemically
947 characterized ‘blue’ and ‘green’ cone photoreceptors in rabbit retina. *Vis. Neurosci.* **12**, 1151–1175
948 (1995).
949 81. Becht, E. *et al.* Dimensionality reduction for visualizing single-cell data using UMAP. *Nat. Biotechnol.*
950 **37**, 38–44 (2019).
951 82. Choi, H. M. T. *et al.* Third-generation in situ hybridization chain reaction: multiplexed, quantitative,
952 sensitive, versatile, robust. *Development* **145**, dev165753 (2018).
953 83. Kimura, Y., Satou, C. & Higashijima, S. V2a and V2b neurons are generated by the final divisions of
954 pair-producing progenitors in the zebrafish spinal cord. *Development* **135**, 3001–3005 (2008).
955 84. Randlett, O. *et al.* Cellular requirements for building a retinal neuropil. *Cell Rep.* **3**, 282–290 (2013).
956 85. Suzuki, S. C. *et al.* Cone photoreceptor types in zebrafish are generated by symmetric terminal
957 divisions of dedicated precursors. *Proc. Natl. Acad. Sci.* **110**, 15109–15114 (2013).
958 86. Kölsch, Y. *et al.* Molecular classification of zebrafish retinal ganglion cells links genes to cell types to
959 behavior. *Neuron* **109**, 645-662.e9 (2021).
960 87. La Manno, G. *et al.* RNA velocity of single cells. *Nature* **560**, 494–498 (2018).
961 88. Hafemeister, C. & Satija, R. Normalization and variance stabilization of single-cell RNA-seq data
962 using regularized negative binomial regression. *Genome Biol.* **20**, 296 (2019).
963 89. Bernardos, R. L., Barthel, L. K., Meyers, J. R. & Raymond, P. A. Late-Stage Neuronal Progenitors in
964 the Retina Are Radial Müller Glia That Function as Retinal Stem Cells. *J. Neurosci.* **27**, 7028–7040
965 (2007).
966 90. Hörnberg, H. *et al.* RNA-binding protein Hermes/RBPMS inversely affects synapse density and axon
967 arbor formation in retinal ganglion cells in vivo. *J. Neurosci. Off. J. Soc. Neurosci.* **33**, 10384–10395
968 (2013).

969 91. Sandell, J. H., Martin, S. C. & Heinrich, G. The development of GABA immunoreactivity in the retina
970 of the zebrafish (Brachydanio rerio). *J. Comp. Neurol.* **345**, 596–601 (1994).
971 92. Abalo, X. M. *et al.* Circadian regulation of phosphodiesterase 6 genes in zebrafish differs between
972 cones and rods: Implications for photopic and scotopic vision. *Vision Res.* **166**, 43–51 (2020).
973 93. Kolosov, D., Bui, P., Chasiotis, H. & Kelly, S. P. Claudins in teleost fishes. *Tissue Barriers* **1**, e25391
974 (2013).
975 94. Kwan, K. M. *et al.* The Tol2kit: A multisite gateway-based construction kit forTol2 transposon
976 transgenesis constructs. *Dev. Dyn.* **236**, 3088–3099 (2007).
977 95. Morris, A. C., Scholz, T. L., Brockerhoff, S. E. & Fadool, J. M. Genetic Dissection Reveals Two Separate
978 Pathways for Rod and Cone Regeneration in the Teleost Retina. *Dev. Neurobiol.* **68**, 605–619 (2008).
979 96. Huang, Y.-Y., Haug, M. F., Gesemann, M. & Neuhauss, S. C. F. Novel Expression Patterns of
980 Metabotropic Glutamate Receptor 6 in the Zebrafish Nervous System. *PLOS ONE* **7**, e35256 (2012).
981